Mastriani *EPJ Quantum Technology* (2023) 10:14
https://doi.org/10.1140/epjqt/s40507-023-00168-z

EPJ Quantum Technology
a SpringerOpen Journal

RESEARCH Open Access

Non-ambiguous and simplified quantum teleportation protocol

Mario Mastriani[1*]

*Correspondence:
mmastria@fiu.edu
[1]Knight Foundation School of Computing & Information Sciences, Florida International University, 11200 S.W. 8th Street, Miami, FL 33199, USA

Abstract

In this study, a new version of the quantum teleportation protocol is presented, which does not require a Bell state measurement (BSM) module on the sender side (Alice), a unitary transform to reconstruct the teleported state on the receiver side (Bob), neither a disambiguation process through two classic bits that travel through a classic disambiguation channel located between sender and receiver. The corresponding theoretical deduction of the protocol, as well as the experimental verification of its operation for several examples of qubits through implementation on an optical table, complete the present study. Both the theoretical and experimental outcomes show a marked superiority in the performance of the new protocol over the original version, with more simplicity and lower implementation costs, and identical fidelity in its most complete version.

Keywords: Entanglement; Optical table; Quantum Internet; Teleportation

1 Introduction

Since its appearance in the literature in 1993 [1], the quantum teleportation protocol has become the cornerstone of one of the most important areas within quantum technology [2–4], that is, quantum communications [5–8].

Since its beginnings [1], the use of the quantum teleportation protocol ranges from its original application in quantum communications [9–21], to its function of supporting future optical networks for the distribution of quantum keys. Specifically, in the quantum cryptography context [22, 23], fiber optic cabling for terrestrial implementations of quantum key distribution (QKD) protocols [24–27] requires quantum repeaters every certain number of kilometers [28, 29], which in turn requires a large amount of quantum memory. The problem is that the key is exposed in its passage through the quantum repeater. There are currently two well-defined lines of research in this respect: the first has to do with the development of quantum repeaters that do not require quantum memory, at least not that much, and the second is to replace the same quantum repeaters with some type of implementation based on quantum teleportation [30]. Therefore, any improvement or simplification of the quantum teleportation protocol will be very well received. The present study deals with this, a more efficient simplification of the mentioned protocol with a clear projection over the future Quantum Internet [31–40].

Regardless of the version of the teleportation protocol used, we cannot use it without a classic channel as part of it, although the difference in the use of that channel has to do with the specific function that it performs in each version. While in the original protocol [1] the classical channel is used for disambiguation, that is, transporting two classical bits for this purpose, in the non-ambiguous version the classical channel is used for the synchronization of the measurements carried out by Alice (the sender) and Bob (the receiver). However, the measurement performed by Alice in the proposed version is not implemented via a Bell state measurement (BSM) module [9–21], as in the original version [1], but through one liquid crystal rotatable polarizer [41] or a combination of two free-space electro-optic modulators (EOM) [42] and one fixed horizontal polarizer, which creates and projects the state inducted by Alice (the sender) onto Bob's side (the receiver). Furthermore, Bob does not need to apply any unitary transforms to reconstruct the teleported state. Therefore, a new teleportation protocol that is not subject to such demands, including no need for disambiguation, will be most welcome due to its simpler and lower-cost implementation.

The outline of the paper is as follows: In Sect. 2, a comparative analysis of both versions of the quantum teleportation protocol is presented, i.e., ambiguous, and complete vs non-ambiguous and simplified, including a detailed theoretical deduction of both versions. Section 3 is constituted by the implementation of the novel on an optical table. Section 4 presents a comparative discussion of the outcomes obtained. Finally, Sect. 5 deals with the general conclusions of this study.

2 Quantum teleportation

Both the complete version (original) [1], i.e., the ambiguous one, as well as the simplified version [30] (non-ambiguous), the quantum teleportation protocol required two types of channels in order to carry out its work. The first channel is quantum and is known as EPR, an acronym derived from a famous article written in 1935 by Albert Einstein, Boris Podolsky, and Nathan Rosen [43], where these authors questioned the completeness of Quantum Mechanics [44]. This channel arises from the creation and subsequent distribution of entangled particles, which in our case are photons. The second channel is the classic one [1, 9–21], which, as we have already mentioned before, transports classic disambiguation bits in the original version of the quantum teleportation protocol so that the receiver (Bob) can correctly reconstruct the teleported qubit. However, in the simplified or non-ambiguous version of teleportation, this channel will carry a synchronization signal, which will allow the correct coordination and recovery of the teleported qubit on the receiver side (Bob). In such a way that until Bob does not receive the synchronization signal sent by Alice, he should not measure, since otherwise, Bob would not know if the result obtained is a consequence of the strong measurement carried out by him, or the weak measurement carried out by Alice, and which is due to the projection action exerted by her rotatable polarizer.

Next, we will theoretically deduce both protocols, although in the case of the original version of the quantum teleportation protocol [1], we will only do so up to the point where the ambiguity of the state to be teleported is revealed, which constitutes the central axis around which all this study revolves, and which marks the performance limit between both versions of the quantum teleportation protocol.

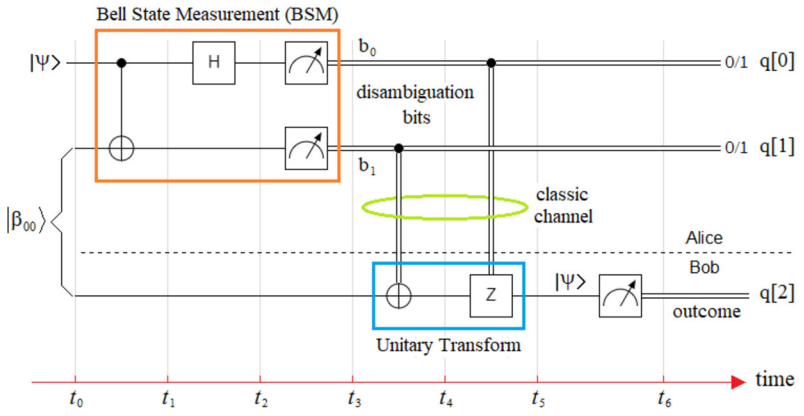

Figure 1 Original, complete, and ambiguous quantum teleportation protocol. Bell state measurement is highlighted in orange on Alice's side; the classic channel between Alice and Bob through which the classic bits $\{b_0, b_1\}$ of disambiguation circulate is highlighted in green; and the unitary transform on Bob's side is highlighted in blue. Single lines represent quantum wires, while double lines represent classical wires

2.1 Ambiguous and complete

Figure 1 represents the original version of the quantum teleportation protocol [1], where there are two well-defined sides divided by a horizontal dot line, the sender (Alice) and the receiver (Bob). On Alice's side, the qubit to be teleported is $|\psi\rangle$, which together with one of the entangled photons enter the Bell State Measurement (BSM). In this case, the Bell state [45] used is,

$$|\beta_{00}\rangle = \big(|00\rangle + |11\rangle\big)/\sqrt{2}, \quad \text{with,} \tag{1}$$

$$|\psi\rangle = \alpha|0\rangle + \beta|1\rangle, \tag{2}$$

where $|\alpha|^2 + |\beta|^2 = 1$, such that $\alpha \wedge \beta \in \mathbb{C}$ of a Hilbert's space [45]. In the most generic case, if we work with electrons, see Fig. A1(a) of Appendix A, we have,

$$\alpha = \cos(\theta/2), \quad \text{and} \tag{3a}$$

$$\beta = e^{i\phi}\sin(\theta/2), \tag{3b}$$

where $0 \leq \theta \leq 2\pi$, and $0 \leq \phi < 2\pi$; however, if we work with photons, see Fig. A1(b) of Appendix A. Thus, we have,

$$\alpha = \cos(\theta), \quad \text{and} \tag{4a}$$

$$\beta = e^{i\phi}\sin(\theta), \tag{4b}$$

where $0 \leq \theta \leq \pi$, and $0 \leq \phi < 2\pi$, although when we work with photons, we do not prepare qubits capriciously oriented in arbitrary directions in space, but with respect to well-defined axes, i.e., the angle ϕ takes values of $\{0; \pi/2; \pi; 3\pi/2\}$ almost exclusively [9–21, 30]. Moreover, for the case of electrons, we have that $|0\rangle = \left[\begin{smallmatrix}1\\0\end{smallmatrix}\right]$ is an *spin-up*, and $|1\rangle = \left[\begin{smallmatrix}0\\1\end{smallmatrix}\right]$ is an *spin-down*, while for the case of photons $|H\rangle = \left[\begin{smallmatrix}1\\0\end{smallmatrix}\right]$ represents the *horizontal polarization*, and $|V\rangle = \left[\begin{smallmatrix}0\\1\end{smallmatrix}\right]$ the *vertical polarization* [45].

In Fig. A1 of the Appendix A, we can appreciate the Bloch sphere for both electrons, and photons (on an optical table). From now on, both in the deductions of the teleportation protocols and in all the experiments related to Sect. 3 carried out on the optical table and considering both the qubit model to be teleported, and the entanglement used (see Appendix B), we will use the Bloch sphere from Fig. A1(b), i.e., for photons.

Returning to Fig. 1, on Alice's side, we can observe a

$$CNOT = \begin{bmatrix} 1 & 0 & 0 & 0 \\ 0 & 1 & 0 & 0 \\ 0 & 0 & 0 & 1 \\ 0 & 0 & 1 & 0 \end{bmatrix}$$

gate [45], a Hadamard $H = \begin{bmatrix} 1/\sqrt{2} & 1/\sqrt{2} \\ 1/\sqrt{2} & -1/\sqrt{2} \end{bmatrix}$ gate [45], and two blocks of strong quantum measurement [46], which together constitute the Bell state measurement (BSM) module [45]. As we will see below, it is precisely in this module where the famous ambiguity of the quantum teleportation protocol [1] is generated. Without the intervention of the strong quantum measurement blocks and in view of the possibility of a violation of the No-Cloning Theorem [47], Bob (the receiver) could never recover the teleported state. Therefore, the strong quantum measurement blocks remove the ambiguity, and at the same time, destroy all possibility of violation of the No-Cloning Theorem by collapsing the wave function [45].

Figure 1 is completed with a classical channel (represented by double lines), which carries the classical bits resulting from the strong quantum measurement performed by Alice, and which represent one of the four possible Bell states [45], that is to say, $|\beta_{00}\rangle = (|00\rangle + |11\rangle)/\sqrt{2}$, $|\beta_{01}\rangle = (|01\rangle + |10\rangle)/\sqrt{2}$, $|\beta_{10}\rangle = (|00\rangle - |11\rangle)/\sqrt{2}$, $|\beta_{11}\rangle = (|01\rangle - |10\rangle)/\sqrt{2}$, which resulted selected as a consequence of the action of the BSM module. On Bob's side, we can see two gates of two qubits each: a CNOT gate and a Control-Z or

$$CZ = \begin{bmatrix} 1 & 0 & 0 & 0 \\ 0 & 1 & 0 & 0 \\ 0 & 0 & 1 & 0 \\ 0 & 0 & 0 & -1 \end{bmatrix}$$

gate, which are activated according to the classical bits received from the classical disambiguation channel, and which constitute the necessary unitary transform for Bob to reconstruct the teleported state [1].

The action of the classical disambiguation channel is key within the quantum teleportation protocol due to two factors. The first concerns the transmission of the classical bits, which will allow Bob to know which unitary transform to prepare in order to successfully reconstruct the teleported state, and the second has to do with being the weak link in the chain, since all the instantaneity of the entanglement is resigned in the teleportation of any state at relativistic speeds [1].

In Appendix C, the complete timeline deduction of this protocol is developed. The last two lines of Equation (C.3), which we reproduce below as Equation (5), are equivalent and highlight the famous ambiguity of the quantum teleportation protocol [1], since the teleported state appears four times in that equation, i.e., there is an overexpression of the state to be teleported when projected onto the four Bell bases at the same time

$\{|\beta_{00}\rangle, |\beta_{01}\rangle, |\beta_{10}\rangle, |\beta_{11}\rangle\}$.

$$\begin{aligned} |\psi(t_2)\rangle &= \big(|00\rangle X^0 Z^0|\psi\rangle + |01\rangle X^1 Z^0|\psi\rangle + |10\rangle X^0 Z^1|\psi\rangle + \big|11\rangle X^1 Z^1|\psi\rangle\big)/2 \\ &\equiv \big(|\beta_{00}\rangle X^0 Z^0|\psi\rangle + |\beta_{01}\rangle X^1 Z^0|\psi\rangle + |\beta_{10}\rangle X^0 Z^1|\psi\rangle + |\beta_{11}\rangle X^1 Z^1|\psi\rangle\big)/2, \end{aligned} \tag{5}$$

where X and Z are defined in Appendix C. This simultaneous projection generates an equiprobable ambiguity, where each Bell base has a 25% chance of being selected as a result of the random action of the BSM module on Alice's side. The BSM module is a strong measurement [45], which resolves the ambiguity by collapsing the wave function and decides things for one of the four Bell bases.

If we now return to Equation (5), we will see that the subscripts of each Bell base match the superscripts of the Pauli matrices X and Z, in such a way that those indices as classical bits travel through the disambiguation channel that connects Alice and Bob in order for Bob to know which gates X and Z to activate to reconstruct the teleported state. The X and Z gates with their respective activation superscripts constitute the unitary transform that Bob must apply to successfully close the teleportation process.

This protocol has presented notable technical implementation challenges during the last decades [9–21] due to the essential coordination of both channels (quantum and classical) to carry out successful teleportation. Therefore, any simplification of this protocol is very welcome.

2.2 Non-ambiguous and simplified

As a generalization of Equation (2) for the case of photons, a generic state to be teleported would be like that of Equation (6),

$$|\psi(\theta,\phi)\rangle = \cos(\theta)|0\rangle + e^{i\phi}\sin(\theta)|1\rangle. \tag{6}$$

Taking this type of qubit as a model, we can construct any of the four Bell states [45], for example the $|\beta_{00}\rangle$ of Equation (7),

$$|\beta_{00}\rangle = \big(\big|\psi(\theta,\phi)\rangle\big|\psi(\theta,\phi)\rangle + \big|\psi(\theta+\pi/2,\phi)\rangle\big|\psi(\theta+\pi/2,\phi)\rangle\big)/\sqrt{2}. \tag{7}$$

However, and in order to simplify the study and subsequent analysis, we prefer to resort to simpler forms of qubits to be teleported, regardless of how generic they are. These simpler forms of generic qubits arise from projections of the state vector $|\psi(\theta,\phi)\rangle$ onto the three planes of the Bloch sphere of Fig. A1(b), i.e., *x*-*y*, *x*-*z*, and *y*-*z*, which can be seen in detail in Appendix B.

Then, from the three qubit models developed in Appendix B, we select the one from Equation (B.2) corresponding to the projection of the state vector $|\psi(\theta,\phi)\rangle$ onto the *x*-*y* plane, which we use to develop the Bell $|\beta_{00}\rangle$ basis of Equation (B.3), that is,

$$|\psi(\theta,0°)\rangle = \cos(\theta)|0\rangle + \sin(\theta)|1\rangle, \quad \text{and} \tag{8}$$

$$|\beta_{00}\rangle = \big(\big|\psi(\theta,0°)\rangle\big|\psi(\theta,0°)\rangle + \big|\psi(\theta+\pi/2,0°)\rangle\big|\psi(\theta+\pi/2,0°)\rangle\big)/\sqrt{2}, \tag{9}$$

whose possible outcomes resulting from the collapse of the wave function common to Alice and Bob, after the weak measurement carried out by the Alice's rotatable polarizer

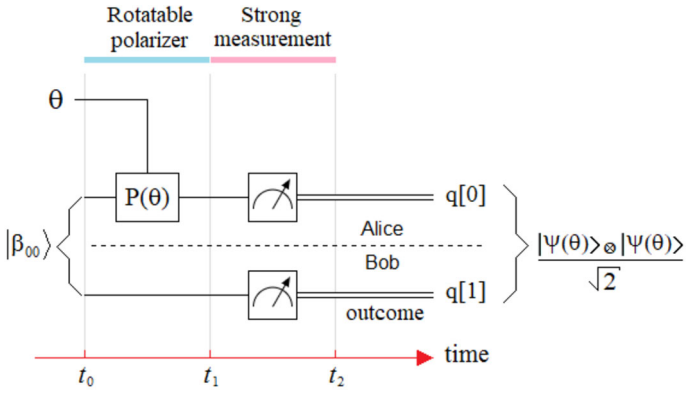

Figure 2 Simplified and non-ambiguous quantum teleportation protocol. The θ angle and the Bell state $|\beta_{00}\rangle$ enter the rotatable polarizer. Two distinct areas correspond to the rotatable polarizer and the strong measurement. The outcomes between the qubits $q[0]$ and $q[1]$ show a 3 dB drop in intensity

of Fig. 2, should be apparently, $|\psi(\theta,0°)\rangle \otimes |\psi(\theta,0°)\rangle$ or $|\psi(\theta+\pi/2,0°)\rangle \otimes |\psi(\theta+\pi/2,0°)\rangle$; however, the rotatable polarizer is strict and always decides in favor of the outcomes of angle θ and not $\theta+\pi/2$ (Fig. 2).

This preliminary analysis begins to hint at a reaction of this protocol against the ambiguities; however, then we will proceed to theoretically verify the aforementioned claim, and later we will do it experimentally on an optical table.

In Appendix D, the complete timeline deduction of this protocol is developed. The last line of Equation (D.5), here reproduced as Equation (10), matches the outcomes of Fig. 2, except for 3 dB, i.e., 50% of the photons survive, since $\frac{1}{\sqrt{2}}\frac{1}{\sqrt{2}} = \frac{1}{2}$. As we will see, this is compensated in practice by an amplifier.

$$|\psi(t_1)\rangle = \frac{|\psi(\theta)\rangle \otimes |\psi(\theta)\rangle}{\sqrt{2}}. \tag{10}$$

What is relevant here is that Alice (the sender) indirectly induces a state like that of Equation (10) at both ends of the EPR channel through entanglement collapse thanks to the action of a rotatable polarizer, which acts as a weak measurement. None of this manifests itself until the intervention of the strong measurement. Alice selects one of the infinitely many possible outcomes internally present in the Bell state of Equation (9) through the correct selection of the angle to be applied to the rotatable polarizer. The replication of a particular state at both ends of the EPR channel, considering the qubit model of Equation (8), is interpreted here as a voluntarily teleported state from Alice to Bob, thanks to the induction of a simultaneous collapse towards that particular state according to the angle of the polarizer. However, this does not imply a violation of the No-Cloning Theorem [47] at all, as explained in Appendix E, since there is no explicit input of a state like that of Equation (8) for its subsequent replication, but an indirect selection of the internal outcomes of the Bell state through a weak measurement process, which coincides with the state that is desired to be shared at both ends.

For this purpose, Alice uses a rotatable polarizer instead of using a BSM as in the original protocol [1], i.e., a weak measurement, although a strong one follows at both ends of the EPR channel.

Another relevant aspect of this protocol is the total absence of ambiguities that must be resolved on Alice's side so that Bob can correctly reconstruct the teleported state. Unlike the original protocol [1], in the version presented here Alice does not have a BSM [46], there are no classic disambiguation bits that tell Bob which type of unitary transform to apply in order to reconstruct the teleported state, given that Bob should not apply any unitary transform to reconstruct that state. However and in principle, we cannot do without the classic channel, which is not used here as part of the disambiguation process, but rather so that Bob knows when to measure, because if Bob measured before Alice applied the polarizer, all teleportation would be distorted, since the state obtained by him would be the typical outcomes presented by the measurement of entanglement [45], and not the desired state. Therefore, a sync signal is sent, from Alice to Bob, through a classical channel. If such synchronism did not exist, Bob would not know whether he is measuring a Bell state of the type in Equation (9) prior to the rotatable polarizer or the post-polarizer state, i.e., the desired state. This uncertainty is dissipated when Bob receives the signal from Alice indicating that the rotatable polarizer was applied, after which he proceeds to make a strong measurement of it [46]. In principle, without the synchronizing signal, Bob does not know if he or Alice trigger the obtaining of the outcomes, and therefore if they are the correct outcomes. Finally, so far, the new protocol has the same degree of uncertainty as the original protocol without the disambiguation bits [1].

3 Implementation on an optical table

Next, we will start with the experimental verification, on the optical table of Fig. 3, of everything demonstrated theoretically in Sect. 2.2. For this purpose, the rotatable polarizer is implemented through the configuration of Equation (D.3), i.e., thanks to two EOMs

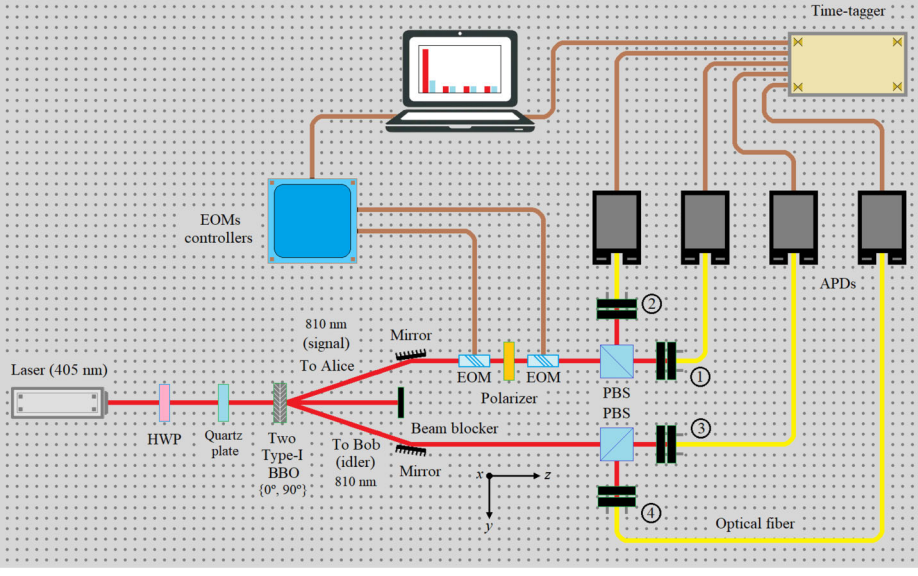

Figure 3 Implementation of the protocol of Fig. 2 on an optical table. The rotatable polarizer is implemented thanks to the $EOM(\theta) + P(0°) + EOM(\theta)$ combination. A pump laser of 405 nm generates two beams of 810 nm at the exit of the BBO crystal. Two polarizing beam splitters with two avalanche photodiodes at the exit of each one complete the layout. A pair of mirrors deflect the beams so that the entire setup is contained on the table without having to resort to fiber optics

[42] with their respective EOMs controllers. For the rest of the protocol implementation of Fig. 2, on the optical table of Fig. 3, we will assume the roles of Alice and Bob at the same time, and for this reason we dispense with the aforementioned synchronization signal and the classical channel. Furthermore, we will prepare simple states to be teleported for easier analysis of the outcomes obtained; however, always respecting the qubit model of Equation (8) for $\theta = \{0°, 90°, 45°, 135°\}$, being $\phi = 0°$.

An input laser beam or pump laser of 405 nm, with a range of power between 20mw and 50 mW, is used as the source of power. In particular, a gallium-nitride (GaN) diode laser is used for two reasons: (i) it has greater stability and temperature control, and (ii) its short wavelength allows us to work with efficient detectors of 810 nm. The blue diode laser beam (405 nm, 50 mW) passes through a zero-order half-wave plate (HWP) with a phase of 22.5°, which represents a Hadamard matrix [45]. Then, the laser beam passes through a narrow bandpass filter or quartz plate of 405 nm. Thanks to this, photons with a state of polarization of diagonal type are obtained,

$$|+\rangle = H|0\rangle = \begin{bmatrix} 1/\sqrt{2} & 1/\sqrt{2} \\ 1/\sqrt{2} & -1/\sqrt{2} \end{bmatrix} \begin{bmatrix} 1 \\ 0 \end{bmatrix} = \begin{bmatrix} 1/\sqrt{2} \\ 1/\sqrt{2} \end{bmatrix}. \tag{11}$$

Later, the laser beam impacts on a solid block ($5 \times 5 \times 3$ mm^3) of beta barium borate (BBO) to produce Type-I down-conversion. Nevertheless, to produce a Bell state of type $|\beta_{00}\rangle$, we use two BBO Type-I crystals (together, one next to the other) rotated by 90°. When $|+\rangle$ enters the first crystal, it generates a pair $|HH\rangle$, while upon entering the second crystal, it generates a pair $|VV\rangle$, in such a way that together both pairs generate the state $|\beta_{00}\rangle$. Using a 405 nm laser pump, this configuration produces a 6° cone at the output of the second crystal, i.e., 3° for the branch known as signal (810 nm) and −3° for the branch known as idler (810 nm), with a phase matching angle for Type-I down-conversion of approximately 29°. In Fig. 3, the angle between both beams (signal and idler) was exaggerated to better appreciate the layout, where the beam path dimensions are not to scale. With the same criteria, several adjustment elements have not been incorporated into Fig. 3 so as not to complicate it.

However, from left to right in Fig. 3, those components are:

- a quartz plate (before BBO) is an $\propto$-BBO, as a phase-matching crystal,
- a BBO, on each beam, after the double BBO, and
- a block of pinhole+filter(808 nm)+lens at the entrance of each avalanche photodiode (APD).

Other elements not yet mentioned will be added in two additional phases called compensation and calibration, which will be explained later along with the components that they require.

Continuing with the implementation of the protocol of Fig. 2 in Fig. 3, both outgoing beams of the second BBO are deflected by two mirrors so that all the geometry of the protocol is completely contained within the useful perimeter of the optical table. A third beam collinear with the beam incident to the first BBO crystal and forming the same angle with the two beams mentioned before (signal, and idler) is intercepted by a beam blocker.

Continuing along Alice's beam, an assembly with one 810 nm calcite film polarizer fixed at horizontal polarization (which is good throughout the visible spectrum and has high

extinction ratios), and two EOMs of 808 nm with controllable angles through two EOM controllers connected to a laptop are used. Two dual-wavelength 405/810 nm polarizing beam-splitter (PBS) of $0.5'' \times 0.5'' \times 0.5''$ are used. When working at 810 nm, the APDs have an efficiency of 60%, and we have worked with acquisition times ranging from 50 ms to 1 sec, with and without a block of pinhole+filter(808 nm)+lens before the APDs. A four-channels time-tagger device is used after the four APDs.

When the state indirectly prepared in the qubit $q[0]$ of Fig. 2, through an angle $\theta = 0°$, is a $|0\rangle$, the outcomes obtained from the optical implementation of Fig. 3 can be seen in the bar graph at the top of Fig. 4, while in case of introducing an angle $\theta = 90°$ in the rotatable polarizer, the state indirectly prepared turns out to be a $|1\rangle$, in which case the outcomes obtained are those of the bar graph at the bottom of Fig. 4. Furthermore, if the θ angle entered into the rotatable polarizer is 45°, the state indirectly prepared will turn out to be $|+\rangle$, and the results obtained can be seen in the upper part of Fig. 5, while for a θ angle = 135°, the state indirectly prepared turns out to be $|-\rangle$, and their corresponding outcomes can be seen at the bottom of Fig. 5, where,

$$\begin{aligned} |-\rangle &= H|1\rangle \\ &= \begin{bmatrix} 1/\sqrt{2} & 1/\sqrt{2} \\ 1/\sqrt{2} & -1/\sqrt{2} \end{bmatrix} \begin{bmatrix} 0 \\ 1 \end{bmatrix} \\ &= \begin{bmatrix} 1/\sqrt{2} \\ -1/\sqrt{2} \end{bmatrix}. \end{aligned} \tag{12}$$

Next, we describe in detail the way in which the performances of Figs. 4 and 5 were obtained according to the protocol of Fig. 3, for which we must take into account that these are relative percentages between APDs of each beam, given that in absolute terms it is necessary to consider the drop of 3 dB present in Equation (D.5), as a consequence of the intervention of the rotatable polarizer. Therefore, we must define the performance of the outcomes obtained with respect to the APDs, both for Alice and Bob in relation to the HV base of both PBS of Fig. 3. Then, Alice's performance with respect to the horizontal output of her PBS results from the photon counting carried out by their respective APDs (1, and 2) is then:

$$\eta_H^A = \frac{n_1}{n_1 + n_2}, \tag{13}$$

while for the case of the vertical output of her PBS, we have,

$$\eta_V^A = \frac{n_2}{n_1 + n_2}, \tag{14}$$

where n_1 represents the result of the photon count in the APD of Alice's exit #1, and n_2 corresponds to the photon count in the APD of Alice's exit #2. With similar criteria, on Bob's side the following performances result,

$$\eta_H^B = \frac{n_3}{n_3 + n_4}, \quad \text{and,} \tag{15}$$

$$\eta_V^B = \frac{n_4}{n_3 + n_4}. \tag{16}$$

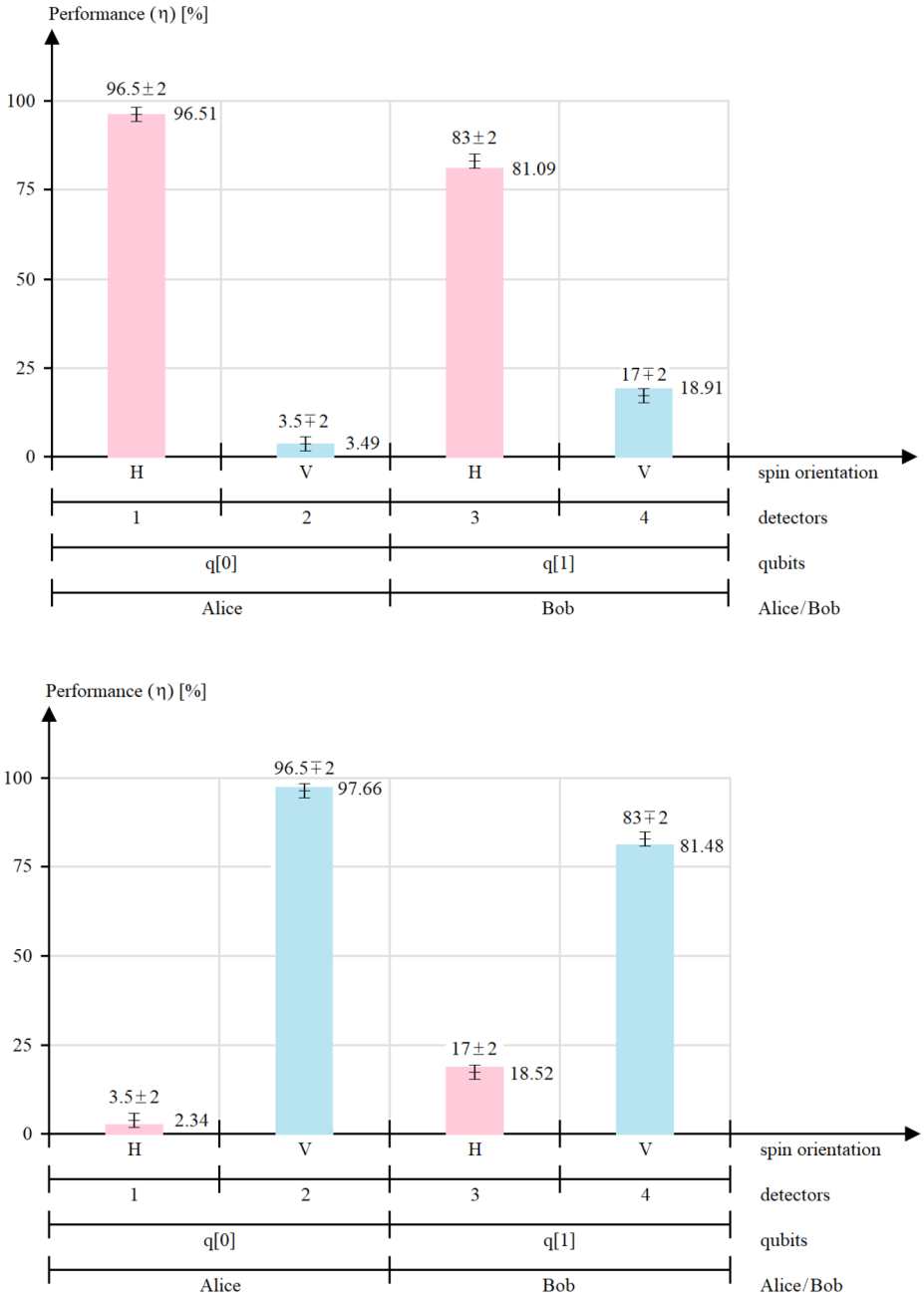

Figure 4 Performance obtained with the optical implementation of Fig. 3. The bar graph at the top corresponds to the case in which the prepared qubit in $q[0]$ is $|0\rangle$, while in the case of preparing a $|1\rangle$, its respective bar graph is at the bottom of this figure. The pink bars correspond to the horizontal polarization performances of qubits $q[0]$ and $q[1]$, while the blue bars correspond to their vertical pola-rization performances. In qubit $q[1]$ on Bob's side, a performance degradation can be distinguished which will be compensated in Sect. 3.1

In this way, we complete Table 1, which confronts the teleported states $\{|0\rangle, |1\rangle, |+\rangle, |-\rangle\}$, and the performances of Equations (13) to (16), expressed numerically in Figs. 4 and 5.

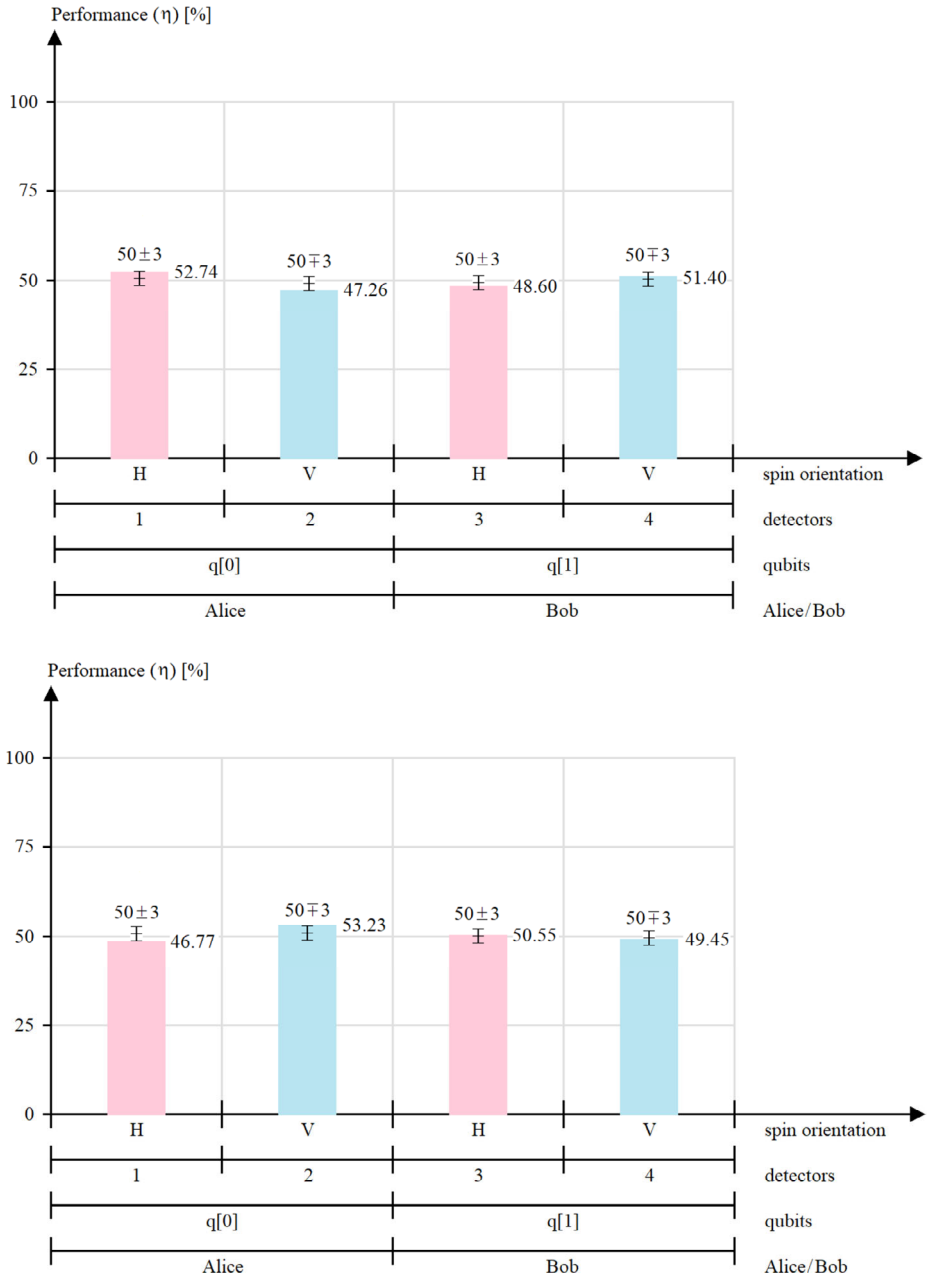

Figure 5 Performance obtained with the optical implementation of Fig. 3. The bar graph at the top corresponds to the case in which the prepared qubit in $q[0]$ is $|+\rangle$, while in the case of preparing a $|-\rangle$, its respective bar graph is at the bottom of this figure. As in Fig. 4, the pink bars correspond to the horizontal polarization performances of qubits $q[0]$ and $q[1]$, while the blue bars correspond to their vertical polarization performances; however, for the teleported states, the degradation of the outcomes on Bob's side that we observed in that figure is not observed here, which indicates the greater affinity for the teleportation of states of the type $\{|+\rangle, |-\rangle\}$ above those of the type $\{|0\rangle, |1\rangle\}$

Based on the performances of Table 1, we will calculate the density matrices of the outcomes of the 3D graphs represented in Fig. 6 for the theoretical ($O^{T}_{|\psi(\theta,0^{\circ})\rangle}$) and experimental ($O^{E}_{|\psi(\theta,0^{\circ})\rangle}$) cases, for which, we must first make explicit the expected outcomes

Table 1 States to teleport $|\psi(\theta,0°)\rangle$ vs their respective performances η

$\|\psi(\theta,0°)\rangle$	η_H^A	η_V^A	η_H^B	η_V^B
$\|0\rangle$	0.9651	0.0349	0.8109	0.1891
$\|1\rangle$	0.0234	0.9766	0.1852	0.8148
$\|+\rangle$	0.5274	0.4726	0.4860	0.5140
$\|-\rangle$	0.4677	0.5323	0.5055	0.4945

and those obtained in each case,

$$O_{|0\rangle}^T = \begin{bmatrix}1\\0\end{bmatrix} \otimes \begin{bmatrix}1\\0\end{bmatrix} = \begin{bmatrix}1\\0\\0\\0\end{bmatrix}, \tag{17}$$

$$O_{|0\rangle}^E = \begin{bmatrix}0.9651\\0.0249\end{bmatrix} \otimes \begin{bmatrix}0.8109\\0.1891\end{bmatrix} = \begin{bmatrix}0.7826\\0.1825\\0.0283\\0.0066\end{bmatrix}, \tag{18}$$

$$\rho_{|0\rangle}^T = \begin{bmatrix}1\\0\\0\\0\end{bmatrix} \begin{bmatrix}1 & 0 & 0 & 0\end{bmatrix} = \begin{bmatrix}1 & 0 & 0 & 0\\0 & 0 & 0 & 0\\0 & 0 & 0 & 0\\0 & 0 & 0 & 0\end{bmatrix}, \quad \text{and} \tag{19}$$

$$\rho_{|0\rangle}^E = \begin{bmatrix}0.7826\\0.1825\\0.0283\\0.0066\end{bmatrix} \begin{bmatrix}0.7826 & 0.1825 & 0.0283 & 0.0066\end{bmatrix}$$

$$= \begin{bmatrix}0.6125 & 0.1428 & 0.0221 & 0.0052\\0.1428 & 0.0333 & 0.0052 & 0.0012\\0.0221 & 0.0052 & 0.0008 & 0.0002\\0.0052 & 0.0012 & 0.0002 & 0\end{bmatrix}, \tag{20}$$

$$O_{|1\rangle}^T = \begin{bmatrix}0\\1\end{bmatrix} \otimes \begin{bmatrix}0\\1\end{bmatrix} = \begin{bmatrix}0\\0\\0\\1\end{bmatrix}, \tag{21}$$

$$O_{|1\rangle}^E = \begin{bmatrix}0.0234\\0.9766\end{bmatrix} \otimes \begin{bmatrix}0.1852\\0.8148\end{bmatrix} = \begin{bmatrix}0.0043\\0.0191\\0.1809\\0.7957\end{bmatrix}, \tag{22}$$

$$\rho_{|1\rangle}^T = \begin{bmatrix}0\\0\\0\\1\end{bmatrix} \begin{bmatrix}0 & 0 & 0 & 1\end{bmatrix} = \begin{bmatrix}0 & 0 & 0 & 0\\0 & 0 & 0 & 0\\0 & 0 & 0 & 0\\0 & 0 & 0 & 1\end{bmatrix}, \quad \text{and} \tag{23}$$

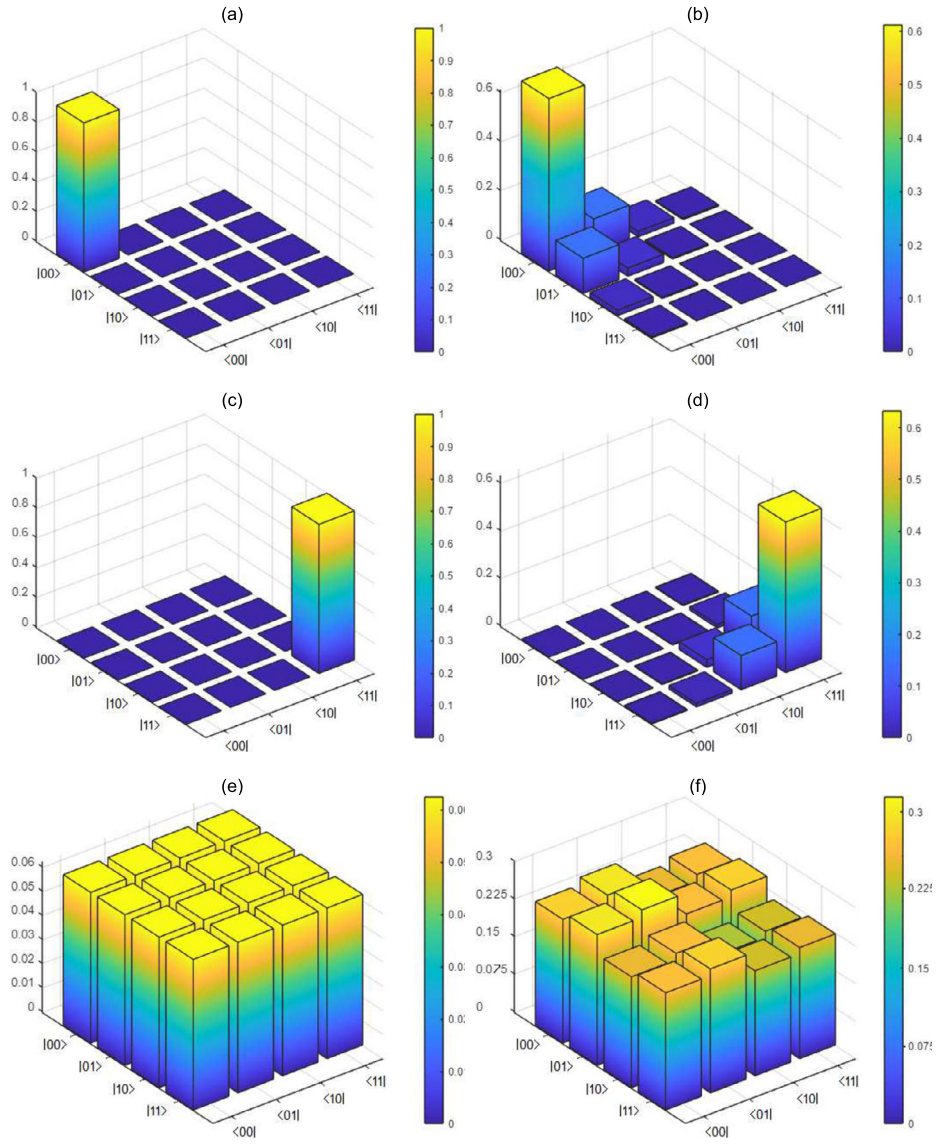

Figure 6 Comparison between the theoretical and the experimental (resulting from the optical implementation of the protocol of Fig. 2) versions of density matrices for the three characteristic examples of states to be teleported, i.e., for: (**a**) $|0\rangle$ theoretical, (**b**) $|0\rangle$ experimental, (**c**) $|1\rangle$ theoretical, (**d**) $|1\rangle$ experimental, (**e**) $|+\rangle$ theoretical, and (**f**) $|+\rangle$ Experimental. The theoretical and experimental results of teleporting the $|-\rangle$ state are not shown so as not to overload the figure. The most notable difference between both versions of the first two cases lies in the existence of non-zero values close to the correct elements, i.e., to those values close to the corners

$$\rho^{E}_{|1\rangle} = \begin{bmatrix} 0.0043 \\ 0.0191 \\ 0.1809 \\ 0.7957 \end{bmatrix} \begin{bmatrix} 0.0043 & 0.0191 & 0.1809 & 0.7957 \end{bmatrix}$$

$$= \begin{bmatrix} 0 & 0.0001 & 0.0008 & 0.0034 \\ 0.0001 & 0.0004 & 0.0034 & 0.0152 \\ 0.0008 & 0.0034 & 0.0327 & 0.1439 \\ 0.0034 & 0.0152 & 0.1439 & 0.6332 \end{bmatrix}, \tag{24}$$

$$O^{T}_{|+\rangle} = \begin{bmatrix} 1/\sqrt{2} \\ 1/\sqrt{2} \end{bmatrix} \otimes \begin{bmatrix} 1/\sqrt{2} \\ 1/\sqrt{2} \end{bmatrix} = \begin{bmatrix} 1/2 \\ 1/2 \\ 1/2 \\ 1/2 \end{bmatrix}, \tag{25}$$

$$O^{E}_{|+\rangle} = \begin{bmatrix} 0.5274 \\ 0.4726 \end{bmatrix} \otimes \begin{bmatrix} 0.4860 \\ 0.5140 \end{bmatrix} = \begin{bmatrix} 0.2563 \\ 0.2711 \\ 0.2297 \\ 0.2429 \end{bmatrix}, \tag{26}$$

with

$$\rho^{T}_{|+\rangle} = \begin{bmatrix} 1/2 \\ 1/2 \\ 1/2 \\ 1/2 \end{bmatrix} \begin{bmatrix} 1/2 & 1/2 & 1/2 & 1/2 \end{bmatrix} = \begin{bmatrix} 1/4 & 1/4 & 1/4 & 1/4 \\ 1/4 & 1/4 & 1/4 & 1/4 \\ 1/4 & 1/4 & 1/4 & 1/4 \\ 1/4 & 1/4 & 1/4 & 1/4 \end{bmatrix}, \quad \text{and} \tag{27}$$

$$\rho^{E}_{|+\rangle} = \begin{bmatrix} 0.2563 \\ 0.2711 \\ 0.2297 \\ 0.2429 \end{bmatrix} \begin{bmatrix} 0.2563 & 0.2711 & 0.2297 & 0.2429 \end{bmatrix}$$

$$= \begin{bmatrix} 0.0657 & 0.0695 & 0.0589 & 0.0623 \\ 0.0695 & 0.0735 & 0.0623 & 0.0659 \\ 0.0589 & 0.0623 & 0.0528 & 0.0558 \\ 0.0623 & 0.0659 & 0.0558 & 0.590 \end{bmatrix}, \tag{28}$$

$$O^{T}_{|-\rangle} = \begin{bmatrix} 1/\sqrt{2} \\ -1/\sqrt{2} \end{bmatrix} \otimes \begin{bmatrix} 1/\sqrt{2} \\ -1/\sqrt{2} \end{bmatrix} = \begin{bmatrix} 1/2 \\ -1/2 \\ -1/2 \\ 1/2 \end{bmatrix}, \tag{29}$$

$$O^{E}_{|-\rangle} = \begin{bmatrix} 0.4677 \\ 0.5323 \end{bmatrix} \otimes \begin{bmatrix} 0.5055 \\ 0.4945 \end{bmatrix} = \begin{bmatrix} 0.2364 \\ 0.2313 \\ 0.2691 \\ 0.2632 \end{bmatrix}, \tag{30}$$

$$\rho^{T}_{|-\rangle} = \begin{bmatrix} 1/2 \\ -1/2 \\ -1/2 \\ 1/2 \end{bmatrix} \begin{bmatrix} 1/2 & -1/2 & -1/2 & 1/2 \end{bmatrix}$$

$$= \begin{bmatrix} 1/4 & -1/4 & -1/4 & 1/4 \\ -1/4 & 1/4 & 1/4 & -1/4 \\ -1/4 & 1/4 & 1/4 & -1/4 \\ 1/4 & -1/4 & -1/4 & 1/4 \end{bmatrix}, \quad \text{and} \tag{31}$$

$$\rho^{E}_{|-\rangle} = \begin{bmatrix} 0.2364 \\ 0.2313 \\ 0.2691 \\ 0.2632 \end{bmatrix} \begin{bmatrix} 0.2364 & 0.2313 & 0.2691 & 0.2632 \end{bmatrix}$$

Table 2 Fidelity in terms of the teleported state $|\psi(\theta,0°)\rangle$

$\|\psi(\theta,0°)\rangle$	$\|0\rangle$	$\|1\rangle$	$\|+\rangle$	$\|-\rangle$
Fidelity	0.8309	0.8348	0.9120	0.9190

$$= \begin{bmatrix} 0.0559 & 0.0547 & 0.0636 & 0.0622 \\ 0.0547 & 0.0535 & 0.0622 & 0.0609 \\ 0.0636 & 0.0622 & 0.0724 & 0.0708 \\ 0.0622 & 0.0699 & 0.0708 & 0.0693 \end{bmatrix}. \tag{32}$$

This last example was not included in Fig. 6 in order not to overload it. Furthermore, with the density matrices of Equations (19), (20), (23), (24), (27), (28), (31), and (32), we will proceed to calculate the respective fidelities corresponding to each example of teleported state, for which, the best definition of fidelity that we can find in the literature is the following [48]: "Fidelity is the measurement of the overlap between two density matrices of theoretical and experimental quantum states obtained as output", and it can be calculated from the following formula,

$$F\left(\rho^T,\rho^E\right) = \left[\mathrm{Tr}\left(\sqrt{\sqrt{\rho^T}\rho^E\sqrt{\rho^T}}\right)\right]^2, \tag{33}$$

where F is the fidelity, Tr(•) means *the trace of a square matrix* (•), ρ^{T} represents the theoretical density matrix of the qubit to be teleported (associated with the sender side), while ρ^{E} is the experimental density matrix resulting from the platform to be used for teleportation (particularly associated with the receiver side). The fidelity of Equation (33) is a widely used expression which possesses a number of valuable properties such as monotonicity under quantum maps, which, in particular, represent the processes of decoherence in real quantum circuits.

Therefore, the fidelities depending on the teleported state $|\psi(\theta,0°)\rangle$ can be seen in Table 2, which clearly shows less distortion in the case of teleporting states of the $\{|+\rangle,|-\rangle\}$ type.

3.1 Compensation phase

As we can see from the experiments carried out in Fig. 3, when Alice wishes to transmit computational basis states (CBS) to Bob, that is to say $\{|0\rangle,|1\rangle\}$, he will receive states of the type: $\{(0.83\pm0.02)|0\rangle + (0.17\mp0.02)|1\rangle, (0.17\pm0.02)|0\rangle + (0.83\mp0.02)|1\rangle\}$, respectively. This can be resolved in the following way, where Bob can perform a post-processing whereby:

- when he gets a $(0.83\pm0.02)|0\rangle + (0.17\mp0.02)|1\rangle \rightarrow \mathrm{post-processing} \rightarrow |0\rangle$, and
- when he gets a $(0.17\pm0.02)|0\rangle + (0.83\mp0.02)|1\rangle \rightarrow \mathrm{post-processing} \rightarrow |1\rangle$,

where the post-processing consists in a logic transpilation inside the laptop of Fig. 3, and the action of the logic transpilation allows, instead of receiving the states mentioned above, he will receive:

- $|0\rangle$, when Alice transmits a $|0\rangle$, and
- $|1\rangle$, when Alice transmits a $|1\rangle$.

In this case, the fidelity inside laptop goes from $(83\pm2)\%$ to 100%.

As we will see in Sect. 4, Fig. 7 shows us that the distortion (difference between the blue and red curves) is greater when $\theta = \{0°,90°\} \leftrightarrow \{|0\rangle,|1\rangle\} = CBS$. This is because it is a much

simpler protocol than the original and is much more directly related to entanglement, which is why the states $\{|+\rangle, |-\rangle\}$ (that is, very well balanced) have almost no distortion.

On the other hand, the distortion analyzed has nothing to do with the 3 dB drop in the outcomes of Equation (10), which is part of the teleportation process of the new protocol. This type of attenuation is also present at the output of the original protocol, which can be observed in Equation (5), where we see that as a result of the action of the BSM the drop is even more pronounced than in the proposed protocol, that is, of 1/2 instead of $1/\sqrt{2}$.

Furthermore, both in the original protocol and in the proposed one, their respective intensity drops do not have to do with a particular θ angle, but affect all of them equally, in such a way that the distinguishability between states can only be compromised if the level of the noise present is very notorious, which is why optical amplifiers must be used to compensate for the aforementioned drops with an excellent signal to noise ratio (SNR).

Finally, in practice, which is especially related to the use of teleportation as an auxiliary of QKD protocols, we are going to work almost exclusively with states of the type $\{|0\rangle, |1\rangle, |+\rangle, |-\rangle\}$, with which the teleportation protocols show the highest performance.

3.2 Calibration phase

The purpose of this phase is to eliminate the classic channel. Therefore, after consulting the manufacturer of the EOMs and the polarizer, and after carrying out several measurements with the GPS clock, we were able to obtain a delay of 0.79 ns generated on Alice's side due to the rotatable polarizer (EOM+Ph+EOM), which was compensated on Bob's side with a free-space optical delay line [49], which works on the basis that the pulses are sent through an optical arrangement with a variable path length, where path lengths in the air are used, which implies a delay of approximately 3.34 ps per millimeter, or approximately 30 cm for a delay of 1 ns.

In this study, and in order to measure the mentioned delay, we use a GPS clock built in our laboratory based on the design of Tony DiCola [50], which uses the Arduino Adafruit METRO 328 Fully Assembled – Arduino IDE compatible – ATmega328 [51].

4 Discussion about the outcomes

As we can see from Table 2, the new protocol shows us that unlike the original version of quantum teleportation [1], the fidelity is better for states of the type $\{|+\rangle, |-\rangle\}$ than in the case of the so-called computational basis states (CBS) [45], i.e., $\{|0\rangle, |1\rangle\}$. This has to do with the fact that the present protocol is more faithful when it comes to teleporting states that are more balanced in their CBS proportions (regardless of the signs that these doses have), than that which is completely unbalanced as the case of a CBS itself.

Next, an evaluation will be carried out about the intervention of the classic channel, which, as we mentioned before, is of main importance in the functional integration of the original protocol [1], while in the new protocol we can dispense with its use by a procedure called *timing calibration*.

In the experiment carried out in Sect. 3 on the optical table, we have fulfilled the role of Alice and Bob at the same time, therefore, the synchronization signal was not necessary, and neither was the classic channel. Since both roles (the sender, and the receiver) were in our charge, we knew when to measure when playing the role of Bob in order to be able to recover the teleported state. However, in a real communication context, where Alice and Bob are separated by a considerable distance and eventually the source of entangled

photons is in the hands of a third actor (e.g., Charlie), we cannot do without the synchronization signal and therefore the classical channel, unless we know exactly both the time it takes for Alice to apply the rotatable polarizer and the time it takes for the photons to travel from the source of entangled photons to the rotatable polarizer. In theory, if the entangled photon source emits anti-bunched photons [52], and we work with a single-photon source and detectors, we could more easily delay Bob's strong measurement until we are sure that when he measures, he will do so after Alice has applied the rotatable polarizer. In this way, calibrating the entire configuration the first time the protocol is used, and sharing information between Alice and Bob through the use of an alternative channel, which by modifying the delay in the application of the strong measurement on Bob's side in a controlled way until full agreement is reached between what Alice says she sent to Bob and what Bob gets by measuring, the calibration of the times of that particular implementation will be successful and consequently the synchronization signal and the classic channel can be dispensed.

Since one of the beams of an entangled pair can be delayed, then Bob's beam should be delayed long enough the first time so that he never measures first. When we have an idea of how long it takes for Alice's infrastructure to apply the rotatable polarizer, as well as the delays in all sections of the distribution of entangled photons via free space [52] or optical fiber [53], we will apply the necessary delay to Bob's beam, through optical configurations specially designed for this purpose [52, 54] or through quantum memories [52], in order to recover the teleported state and thus save ourselves the synchronization signal and the classical channel. Retarding entangled photons is a common practice in the laboratory [52–54]. In cases where the calibration of the times of a quantum communications protocol is critical, a global-position-system (GPS) clock [9, 10] is used to synchronize the times with total precision and accuracy.

In Equation (D.5) of Sect. 2.2, we were able to observe that as a consequence of the action of the rotatable polarizer the outcomes drop by 3 dB, which means that 50% of the photons that were emitted by the source survive, regardless if they were entangled-photons before the rotatable polarizer and independent photons after this. The rotatable polarizer $P(\theta)$ filters and what before it was a normalization of the Bell state $|\beta_{00}\rangle$ of Equation (11) of unitary modulus, after $P(\theta)$ that modulus drops to $1/\sqrt{2}$. The action of $P(\theta)$ is only filtering and its incidence in the 3 dB drop is due to the action of suppressing those components of $|\beta_{00}\rangle$ that are at 90° of the θ angle of $P(\theta)$. In other words, $P(\theta)$ filters, unmasks a reality, and in this way disturbs the original normalization of $|\beta_{00}\rangle$. As we have already mentioned before, this is not a problem since this drop in the module of the outcomes can be compensated with an amplifier.

On the other hand, the drop in the modulus of the outcomes is unavoidable due to several factors: (a) Malus' Law [55], (b) the rotatable polarizer $P(\theta)$ is not a perfect filter, that is, it has absorption losses, and (c) several additional and concomitant factors of lesser incidence, such as reflection, among others. For this reason, the APD #2 (vertical output of the PBS) of Alice in Fig. 4 does not count 0 photons when $P(\theta) = P(0°)$, and it is not a perfect projector either; for this reason the APD #4 (vertical output of the PBS) from Bob also does not count 0 photons when $P(\theta) = P(0°)$. As a consequence of this, the rotatable polarizer does not induce or project accurately. As a consequence of this, post-processing in order to correctly interpret the results is required, such that when Bob gets an outcome of approximately $\{(0.83 \pm 0.02)|0\rangle + (0.17 \mp 0.02)|1\rangle\}$, what Alice really wanted to project

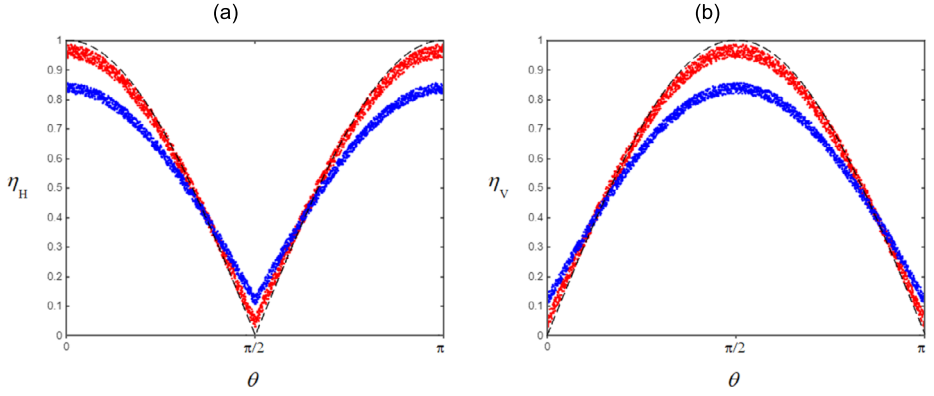

Figure 7 Performances for θ angle between 0 and π: (**a**) η_H^A (red), and η_H^B (blue), and (**b**) η_V^A (red), and η_V^B (blue). In both figures, the dotted black lines represent the ideal case, and ignoring the mentioned losses, near $\theta = \pi/4$, and $3\pi/4$ the three curves, in (**a**) and (**b**), practically coincide. Both in the case of the outcomes detected by the APDs of Alice and in the case of Bob, both figures show us that the performances comply with the following equalities: $\eta_H^A + \eta_V^A = 1$, and $\eta_H^B + \eta_V^B = 1$

was a $|0\rangle$, and when Bob gets an outcome of about $\{(0.17 \mp 0.02)|0\rangle + (0.83 \pm 0.02)|1\rangle\}$, what Alice really wanted to project was a $|1\rangle$. The case of the states $\{|+\rangle, |-\rangle\}$ is different, since as we have seen, when Alice tries to project them, Bob receives them with the highest fidelity.

Finally, Fig. 7(a) shows η_H^A (red), and η_H^B (blue) from Equations (13) and (14) in terms of the θ angle of $P(\theta)$, while Fig. 7(b) shows η_V^A (red), and η_V^B (blue) from Equations (15) and (16) in terms of the θ angle of $P(\theta)$, when the θ angle of the EOMs that implement the rotatable polarizer varies between 0 and π. In both figures, the dotted black lines represent the ideal case. As can be seen, the aforementioned post-processing is required mainly when Alice wants to project states of the type $\{|0\rangle, |1\rangle\}$, which together with the states $\{|+\rangle, |-\rangle\}$ are those that have been to teleport in 100% of the cases, since there are no practical examples that justify the teleportation of states with capricious orientations on the Bloch sphere.

5 Conclusions

A simplified and non-ambiguous version of the quantum teleportation protocol has been presented. Both the theoretical deduction and the experimental verification of the outcomes on an optical table have demonstrated the feasibility of this new and performant version.

Based on the qubit model of Equation (8) and the deduction of the Bell state $|\beta_{00}\rangle$ of Equation (9) from that model, we have shown that the intervention of a weak measurement carried out by means of a rotatable polarizer on Alice's side (the sender) induces or projects a desired state on Bob's side (the receiver), which is interpreted in the context of this new protocol as the teleportation of an underlying state hinted at through the θ angle according to the selected qubit model.

Notwithstanding the qubit model selected to carry out the experiments in Sect. 3, all the qubit models in Appendix B have been successfully tested on an optical table.

As shown in Appendix E, the protocol in Fig. 2 does not violate the No-Cloning Theorem, since there is no incoming state to that protocol that is replicated at its output, but

rather a pair of incoming angles, where θ is a variable and ϕ is a parameter, i.e., we apply *ceteris paribus*.

The 3 dBs drop in outcomes seen in Equation (D.5) of Sect. 2.2 is not a problem at all, since it can be compensated for with an amplifier. However, this protocol requires post-processing of the outcomes on Bob's (the receiver) side for the correct interpretation of the states projected by Alice (the sender).

Finally, the possibility of removing the classic channel after a timing calibration procedure, further projects the new protocol to replace quantum repeaters [28, 29] in QKD infrastructures [24–27], and in the future Quantum Internet [31–40].

Appendix A: Bloch's spheres

In Fig. A1, we can appreciate two Bloch's spheres. Figure A1(a) shows the one used in the case of electrons, while Fig. A1(b) presents the sphere used in the case of photons on an optical table. In the case of Fig. A1(a), we speak of spin-up or spin-$|0\rangle$ for those states located at the north pole of the sphere, and of spin-down or spin-$|1\rangle$ for states located at the south pole of it. Comparing both figures, it is possible to appreciate that for both electrons and photons (on an optical table), although we use θ as the angle that takes us from one state to another, in the case of electrons that angle starts on the z axis and descends, while in the case of photons, this angle starts in the x-y plane and goes up. This naming is key in the analysis of the configuration of the experiments carried out on the optical table in Sect. 3, according to the model of the qubit to be teleported and the entanglement used, which was developed in Appendix B.

In Fig. A1(b), the entangled (unpolarized) photon advances in the z-direction (entering the page) in such a way that it leaves behind the source of entangled photons and will impact ahead with the optical devices that are part of the teleportation protocol implemented.

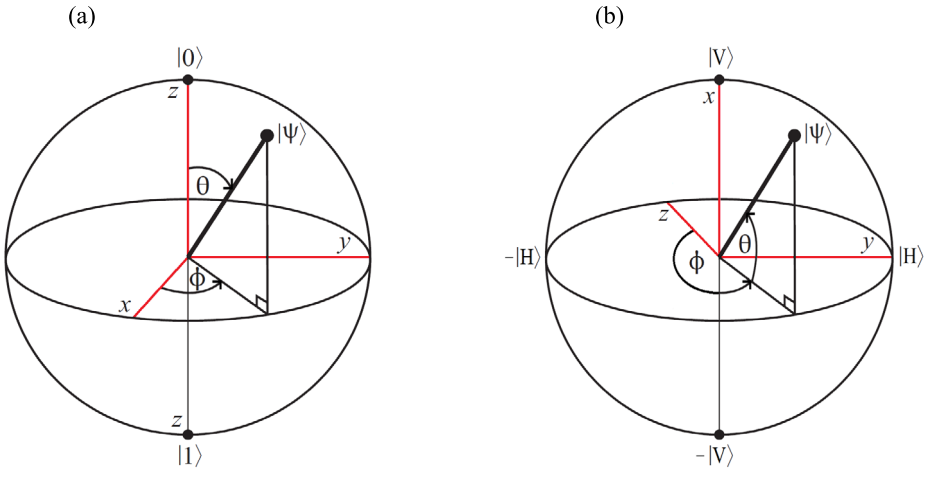

Figure A1 Bloch sphere of a qubit for: (**a**) electrons, and (**b**) photons on an optical table, where the source of entangled photons is behind and the polarizers/detectors are ahead

Appendix B: Bell bases from qubits projected onto planes of the Bloch's sphere

Given the qubit model to be teleported for the photons case,

$$|\psi(\theta,\phi)\rangle = \cos(\theta)|0\rangle + e^{i\phi}\sin(\theta)|1\rangle, \tag{B.1}$$

and according to which one of the three planes in Fig. A1(b) the entanglement used is developed, we will have a complete set of the four Bell bases [45], according to that plane.

1. *Entanglement in the x-z plane of Fig.* A1(b), *where* $\phi = 0°$, *and* θ *can vary freely:*
   Then the model of qubit results,

$$|\psi(\theta,0°)\rangle = \cos(\theta)|0\rangle + \sin(\theta)|1\rangle. \tag{B.2}$$

In terms of this model of qubit the four Bell states arise:

$$\begin{aligned}|\beta_{00}\rangle &= \big(|\psi(\theta,0°)\rangle|\psi(\theta,0°)\rangle + |\psi(\theta+\pi/2,0°)\rangle|\psi(\theta+\pi/2,0°)\rangle\big)/\sqrt{2}\\ &= \big(\big(\cos(\theta)|0\rangle + \sin(\theta)|1\rangle\big)\big(\cos(\theta)|0\rangle + \sin(\theta)|1\rangle\big)\\ &\quad + \big(\cos(\theta+\pi/2)|0\rangle + \sin(\theta+\pi/2)|1\rangle\big)\big(\cos(\theta+\pi/2)|0\rangle\\ &\quad + \sin(\theta+\pi/2)|1\rangle\big)\big)/\sqrt{2}.\end{aligned} \tag{B.3}$$

Now, being,

$$\cos(\theta+\pi/2) = -\sin(\theta), \quad \text{and} \tag{B.4a}$$

$$\sin(\theta+\pi/2) = \cos(\theta), \tag{B.4b}$$

if we replace Equations (B.4a) and (B.4b) into Equation (B.3), the latter results,

$$\begin{aligned}|\beta_{00}\rangle &= \big(\big(\cos(\theta)|0\rangle + \sin(\theta)|1\rangle\big)\big(\cos(\theta)|0\rangle + \sin(\theta)|1\rangle\big)\\ &\quad + \big(-\sin(\theta)|0\rangle + \cos(\theta)|1\rangle\big)\big(-\sin(\theta)|0\rangle + \cos(\theta)|1\rangle\big)\big)/\sqrt{2}\\ &= \big(\cos(\theta)^2|00\rangle + \sin(\theta)\cos(\theta)|10\rangle + \cos(\theta)\sin(\theta)|01\rangle + \sin(\theta)^2|11\rangle\\ &\quad + \sin(\theta)^2|00\rangle - \sin(\theta)\cos(\theta)|10\rangle - \cos(\theta)\sin(\theta)|01\rangle + \cos(\theta)^2|11\rangle\big)/\sqrt{2}\\ &= \big(|00\rangle + |11\rangle\big)/\sqrt{2}.\end{aligned} \tag{B.5}$$

Considering the inverter Pauli gate $X = \left[\begin{smallmatrix}0 & 1\\ 1 & 0\end{smallmatrix}\right]$, such as $X|0\rangle = |1\rangle$ and $X|1\rangle = |0\rangle$, $I_{2\times 2} = \left[\begin{smallmatrix}1 & 0\\ 0 & 1\end{smallmatrix}\right]$, and also Equation (B.4a)–(B.4b), yields

$$\begin{aligned}|\beta_{01}\rangle &= (X + I_{2\times 2})|\beta_{00}\rangle\\ &= \big(X|\psi(\theta,0°)\rangle|\psi(\theta,0°)\rangle + X|\psi(\theta+\pi/2,0°)\rangle|\psi(\theta+\pi/2,0°)\rangle\big)/\sqrt{2}\\ &= \big(X\big(\cos(\theta)|0\rangle + \sin(\theta)|1\rangle\big)\big(\cos(\theta)|0\rangle + \sin(\theta)|1\rangle\big)\\ &\quad + X\big(\cos(\theta+\pi/2)|0\rangle + \sin(\theta+\pi/2)|1\rangle\big)\\ &\quad \times \big(\cos(\theta+\pi/2)|0\rangle + \sin(\theta+\pi/2)|1\rangle\big)\big)/\sqrt{2}\\ &= \big(\big(\cos(\theta)X|0\rangle + \sin(\theta)X|1\rangle\big)\big(\cos(\theta)|0\rangle + \sin(\theta)|1\rangle\big)\end{aligned}$$

$$
\begin{aligned}
&+\big(\cos(\theta+\pi/2)X|0\rangle+\sin(\theta+\pi/2)X|1\rangle\big)\\
&\times\big(\cos(\theta+\pi/2)|0\rangle+\sin(\theta+\pi/2)|1\rangle\big)\big)/\sqrt{2}\\
=&\big(\big(\cos(\theta)|1\rangle+\sin(\theta)|0\rangle\big)\big(\cos(\theta)|0\rangle+\sin(\theta)|1\rangle\big)\\
&+\big(\cos(\theta+\pi/2)|1\rangle+\sin(\theta+\pi/2)|0\rangle\big)\\
&\times\big(\cos(\theta+\pi/2)|0\rangle+\sin(\theta+\pi/2)|1\rangle\big)\big)/\sqrt{2}\\
=&\big(\big(\cos(\theta)|1\rangle+\sin(\theta)|0\rangle\big)\big(\cos(\theta)|0\rangle+\sin(\theta)|1\rangle\big)\\
&+\big(-\sin(\theta)|1\rangle+\cos(\theta)|0\rangle\big)\big(-\sin(\theta)|0\rangle+\cos(\theta)|1\rangle\big)\big)/\sqrt{2}\\
=&\big(\cos(\theta)^2|10\rangle+\sin(\theta)\cos(\theta)|00\rangle+\cos(\theta)\sin(\theta)|11\rangle+\sin(\theta)^2|01\rangle\\
&+\sin(\theta)^2|10\rangle-\sin(\theta)\cos(\theta)|00\rangle-\cos(\theta)\sin(\theta)|11\rangle+\cos(\theta)^2|01\rangle\big)/\sqrt{2}\\
=&\big(|01\rangle+|10\rangle\big)/\sqrt{2}.
\end{aligned}
\tag{B.6}
$$

Now, considering $Z=\left[\begin{smallmatrix}1&0\\0&-1\end{smallmatrix}\right]$, where $Z|0\rangle=|0\rangle$, and $Z|1\rangle=-|1\rangle$, results,

$$
\begin{aligned}
|\beta_{10}\rangle=&(Z+I_{2\times2})|\beta_{00}\rangle\\
=&\big(Z\big|\psi(\theta,0^\circ)\big\rangle\big|\psi(\theta,0^\circ)\big\rangle+Z\big|\psi(\theta+\pi/2,0^\circ)\big\rangle\big|\psi(\theta+\pi/2,0^\circ)\big\rangle\big)/\sqrt{2}\\
=&\big(Z\big(\cos(\theta)|0\rangle+\sin(\theta)|1\rangle\big)\big(\cos(\theta)|0\rangle+\sin(\theta)|1\rangle\big)\\
&+Z\big(\cos(\theta+\pi/2)|0\rangle+\sin(\theta+\pi/2)|1\rangle\big)\\
&\times\big(\cos(\theta+\pi/2)|0\rangle+\sin(\theta+\pi/2)|1\rangle\big)\big)/\sqrt{2}\\
=&\big(\big(\cos(\theta)Z|0\rangle+\sin(\theta)Z|1\rangle\big)\big(\cos(\theta)|0\rangle+\sin(\theta)|1\rangle\big)\\
&+\big(\cos(\theta+\pi/2)Z|0\rangle+\sin(\theta+\pi/2)Z|1\rangle\big)\\
&\times\big(\cos(\theta+\pi/2)|0\rangle+\sin(\theta+\pi/2)|1\rangle\big)\big)/\sqrt{2}\\
=&\big(\big(\cos(\theta)|0\rangle-\sin(\theta)|1\rangle\big)\big(\cos(\theta)|0\rangle+\sin(\theta)|1\rangle\big)\\
&+\big(\cos(\theta+\pi/2)|0\rangle-\sin(\theta+\pi/2)|1\rangle\big)\\
&\times\big(\cos(\theta+\pi/2)|0\rangle+\sin(\theta+\pi/2)|1\rangle\big)\big)/\sqrt{2}\\
=&\big(\big(\cos(\theta)|0\rangle-\sin(\theta)|1\rangle\big)\big(\cos(\theta)|0\rangle+\sin(\theta)|1\rangle\big)\\
&+\big(-\sin(\theta)|0\rangle-\cos(\theta)|1\rangle\big)\big(-\sin(\theta)|0\rangle+\cos(\theta)|1\rangle\big)\big)/\sqrt{2}\\
=&\big(\cos(\theta)^2|00\rangle-\sin(\theta)\cos(\theta)|10\rangle+\cos(\theta)\sin(\theta)|01\rangle-\sin(\theta)^2|11\rangle\\
&+\sin(\theta)^2|00\rangle+\sin(\theta)\cos(\theta)|10\rangle-\cos(\theta)\sin(\theta)|01\rangle-\cos(\theta)^2|11\rangle\big)/\sqrt{2}\\
=&\big(|00\rangle-|11\rangle\big)/\sqrt{2}.
\end{aligned}
\tag{B.7}
$$

While,

$$
\begin{aligned}
|\beta_{11}\rangle=&(ZX+I_{2\times2})|\beta_{00}\rangle\\
=&\big(ZX\big|\psi(\theta,0^\circ)\big\rangle\big|\psi(\theta,0^\circ)\big\rangle+ZX\big|\psi(\theta+\pi/2,0^\circ)\big\rangle\big|\psi(\theta+\pi/2,0^\circ)\big\rangle\big)/\sqrt{2}\\
=&\big(ZX\big(\cos(\theta)|0\rangle+\sin(\theta)|1\rangle\big)\big(\cos(\theta)|0\rangle+\sin(\theta)|1\rangle\big)
\end{aligned}
$$

$$
\begin{aligned}
&+ ZX\big(\cos(\theta+\pi/2)|0\rangle + \sin(\theta+\pi/2)|1\rangle\big)\\
&\times \big(\cos(\theta+\pi/2)|0\rangle + \sin(\theta+\pi/2)|1\rangle\big)\big)/\sqrt{2}\\
&= \big(\big(\cos(\theta)ZX|0\rangle + \sin(\theta)ZX|1\rangle\big)\big(\cos(\theta)|0\rangle + \sin(\theta)|1\rangle\big)\\
&+ \big(\cos(\theta+\pi/2)ZX|0\rangle + \sin(\theta+\pi/2)ZX|1\rangle\big)\\
&\times \big(\cos(\theta+\pi/2)|0\rangle + \sin(\theta+\pi/2)|1\rangle\big)\big)/\sqrt{2}\\
&= \big(\big(-\cos(\theta)|1\rangle + \sin(\theta)|0\rangle\big)\big(\cos(\theta)|0\rangle + \sin(\theta)|1\rangle\big)\\
&+ \big(-\cos(\theta+\pi/2)|1\rangle + \sin(\theta+\pi/2)|0\rangle\big)\\
&\times \big(\cos(\theta+\pi/2)|0\rangle + \sin(\theta+\pi/2)|1\rangle\big)\big)/\sqrt{2}\\
&= \big(\big(-\cos(\theta)|1\rangle + \sin(\theta)|0\rangle\big)\big(\cos(\theta)|0\rangle + \sin(\theta)|1\rangle\big)\\
&+ \big(\sin(\theta)|1\rangle + \cos(\theta)|0\rangle\big)\big(-\sin(\theta)|0\rangle + \cos(\theta)|1\rangle\big)\big)/\sqrt{2}\\
&= \big(-\cos(\theta)^2|10\rangle + \sin(\theta)\cos(\theta)|00\rangle - \cos(\theta)\sin(\theta)|11\rangle + \sin(\theta)^2|01\rangle\\
&- \sin(\theta)^2|10\rangle - \sin(\theta)\cos(\theta)|00\rangle + \cos(\theta)\sin(\theta)|11\rangle + \cos(\theta)^2|01\rangle\big)/\sqrt{2}\\
&= \big(|01\rangle - |10\rangle\big)/\sqrt{2}. \qquad \text{(B.8)}
\end{aligned}
$$

2. *Entanglement in the z-y plane of Fig.* A1(b), *where* $\phi = \pi/2$, *and* θ *can vary freely:* Then the model of qubit results,

$$|\psi(\theta,\pi/2)\rangle = \cos(\theta)|0\rangle + i\sin(\theta)|1\rangle, \quad \text{and} \qquad \text{(B.9a)}$$

$$|\overline{\psi}(\theta,\pi/2)\rangle = \cos(\theta)|0\rangle - i\sin(\theta)|1\rangle, \qquad \text{(B.9b)}$$

where $i = \sqrt{-1}$. Then, in terms of this model of qubit the four Bell states arise:

$$
\begin{aligned}
|\beta_{00}\rangle &= \big(|\overline{\psi}(\theta,0^\circ)\rangle|\psi(\theta,0^\circ)\rangle + |\overline{\psi}(\theta+\pi/2,0^\circ)\rangle|\psi(\theta+\pi/2,0^\circ)\rangle\big)/\sqrt{2}\\
&= \big(\big(\cos(\theta)|0\rangle - i\sin(\theta)|1\rangle\big)\big(\cos(\theta)|0\rangle + i\sin(\theta)|1\rangle\big)\\
&+ \big(\cos(\theta+\pi/2)|0\rangle - i\sin(\theta+\pi/2)|1\rangle\big)\\
&\times \big(\cos(\theta+\pi/2)|0\rangle + i\sin(\theta+\pi/2)|1\rangle\big)\big)/\sqrt{2}\\
&= \big(\big(\cos(\theta)|0\rangle - i\sin(\theta)|1\rangle\big)\big(\cos(\theta)|0\rangle + i\sin(\theta)|1\rangle\big)\\
&+ \big(-\sin(\theta)|0\rangle - i\cos(\theta)|1\rangle\big)\big(-\sin(\theta)|0\rangle + i\cos(\theta)|1\rangle\big)\big)/\sqrt{2}\\
&= \big(\cos(\theta)^2|00\rangle - i\sin(\theta)\cos(\theta)|10\rangle + i\cos(\theta)\sin(\theta)|01\rangle + \sin(\theta)^2|11\rangle\\
&+ \sin(\theta)^2|00\rangle + i\sin(\theta)\cos(\theta)|10\rangle - i\cos(\theta)\sin(\theta)|01\rangle + \cos(\theta)^2|11\rangle\big)/\sqrt{2}\\
&= \big(|00\rangle + |11\rangle\big)/\sqrt{2}, \qquad \text{(B.10)}\\
|\beta_{01}\rangle &= (X + I_{2\times 2})|\beta_{00}\rangle\\
&= \big(X|\overline{\psi}(\theta,0^\circ)\rangle|\psi(\theta,0^\circ)\rangle + X|\overline{\psi}(\theta+\pi/2,0^\circ)\rangle|\psi(\theta+\pi/2,0^\circ)\rangle\big)/\sqrt{2}\\
&= \big(X\big(\cos(\theta)|0\rangle - i\sin(\theta)|1\rangle\big)\big(\cos(\theta)|0\rangle + i\sin(\theta)|1\rangle\big)\\
&+ X\big(\cos(\theta+\pi/2)|0\rangle - i\sin(\theta+\pi/2)|1\rangle\big)
\end{aligned}
$$

$$
\begin{aligned}
&\times \big(\cos(\theta+\pi/2)|0\rangle + i\sin(\theta+\pi/2)|1\rangle\big)\big)/\sqrt{2}\\
&= \Big(\big(\cos(\theta)X|0\rangle - i\sin(\theta)X|1\rangle\big)\big(\cos(\theta)|0\rangle + i\sin(\theta)|1\rangle\big)\\
&\quad + \big(\cos(\theta+\pi/2)X|0\rangle - i\sin(\theta+\pi/2)X|1\rangle\big)\\
&\quad \times \big(\cos(\theta+\pi/2)|0\rangle + i\sin(\theta+\pi/2)|1\rangle\big)\Big)/\sqrt{2}\\
&= \Big(\big(\cos(\theta)|1\rangle - i\sin(\theta)|0\rangle\big)\big(\cos(\theta)|0\rangle + i\sin(\theta)|1\rangle\big)\\
&\quad + \big(\cos(\theta+\pi/2)|1\rangle - i\sin(\theta+\pi/2)|0\rangle\big)\\
&\quad \times \big(\cos(\theta+\pi/2)|0\rangle + i\sin(\theta+\pi/2)|1\rangle\big)\Big)/\sqrt{2}\\
&= \Big(\big(\cos(\theta)|1\rangle - i\sin(\theta)|0\rangle\big)\big(\cos(\theta)|0\rangle + i\sin(\theta)|1\rangle\big)\\
&\quad + \big(-\sin(\theta)|1\rangle - i\cos(\theta)|0\rangle\big)\big(-\sin(\theta)|0\rangle + i\cos(\theta)|1\rangle\big)\Big)/\sqrt{2}\\
&= \big(\cos(\theta)^2|10\rangle - i\sin(\theta)\cos(\theta)|00\rangle + i\cos(\theta)\sin(\theta)|11\rangle + \sin(\theta)^2|01\rangle\\
&\quad + \sin(\theta)^2|10\rangle + i\sin(\theta)\cos(\theta)|00\rangle - i\cos(\theta)\sin(\theta)|11\rangle + \cos(\theta)^2|01\rangle\big)/\sqrt{2}\\
&= \big(|01\rangle + |10\rangle\big)/\sqrt{2}, \qquad \text{(B.11)}
\end{aligned}
$$

$$
\begin{aligned}
|\beta_{10}\rangle &= (Z + I_{2\times 2})|\beta_{00}\rangle\\
&= \big(Z\big|\overline{\psi}(\theta,0^\circ)\big\rangle\big|\psi(\theta,0^\circ)\big\rangle + Z\big|\overline{\psi}(\theta+\pi/2,0^\circ)\big\rangle\big|\psi(\theta+\pi/2,0^\circ)\big\rangle\big)/\sqrt{2}\\
&= \Big(Z\big(\cos(\theta)|0\rangle - i\sin(\theta)|1\rangle\big)\big(\cos(\theta)|0\rangle + i\sin(\theta)|1\rangle\big)\\
&\quad + Z\big(\cos(\theta+\pi/2)|0\rangle - i\sin(\theta+\pi/2)|1\rangle\big)\\
&\quad \times \big(\cos(\theta+\pi/2)|0\rangle + i\sin(\theta+\pi/2)|1\rangle\big)\Big)/\sqrt{2}\\
&= \Big(\big(\cos(\theta)Z|0\rangle - i\sin(\theta)Z|1\rangle\big)\big(\cos(\theta)|0\rangle + i\sin(\theta)|1\rangle\big)\\
&\quad + \big(\cos(\theta+\pi/2)Z|0\rangle - i\sin(\theta+\pi/2)Z|1\rangle\big)\\
&\quad \times \big(\cos(\theta+\pi/2)|0\rangle + i\sin(\theta+\pi/2)|1\rangle\big)\Big)/\sqrt{2}\\
&= \Big(\big(\cos(\theta)|0\rangle + i\sin(\theta)|1\rangle\big)\big(\cos(\theta)|0\rangle + i\sin(\theta)|1\rangle\big)\\
&\quad + \big(\cos(\theta+\pi/2)|0\rangle + i\sin(\theta+\pi/2)|1\rangle\big)\\
&\quad \times \big(\cos(\theta+\pi/2)|0\rangle + i\sin(\theta+\pi/2)|1\rangle\big)\Big)/\sqrt{2}\\
&= \Big(\big(\cos(\theta)|0\rangle + i\sin(\theta)|1\rangle\big)\big(\cos(\theta)|0\rangle + i\sin(\theta)|1\rangle\big)\\
&\quad + \big(-\sin(\theta)|0\rangle + i\cos(\theta)|1\rangle\big)\big(-\sin(\theta)|0\rangle + i\cos(\theta)|1\rangle\big)\Big)/\sqrt{2}\\
&= \big(\cos(\theta)^2|00\rangle + i\sin(\theta)\cos(\theta)|10\rangle + i\cos(\theta)\sin(\theta)|01\rangle - \sin(\theta)^2|11\rangle\\
&\quad + \sin(\theta)^2|00\rangle - i\sin(\theta)\cos(\theta)|10\rangle - i\cos(\theta)\sin(\theta)|01\rangle - \cos(\theta)^2\big|11\rangle\big)/\sqrt{2}\\
&= \big(|00\rangle - |11\rangle\big)/\sqrt{2}, \qquad \text{(B.12)}
\end{aligned}
$$

$$
\begin{aligned}
|\beta_{11}\rangle &= (ZX + I_{2\times 2})|\beta_{00}\rangle\\
&= \big(ZX\big|\overline{\psi}(\theta,0^\circ)\big\rangle\big|\psi(\theta,0^\circ)\big\rangle + ZX\big|\overline{\psi}(\theta+\pi/2,0^\circ)\big\rangle\big|\psi(\theta+\pi/2,0^\circ)\big\rangle\big)/\sqrt{2}\\
&= \Big(ZX\big(\cos(\theta)|0\rangle - i\sin(\theta)|1\rangle\big)\big(\cos(\theta)\big|0\rangle + i\sin(\theta)|1\rangle\big)\\
&\quad + ZX\big(\cos(\theta+\pi/2)|0\rangle - i\sin(\theta+\pi/2)|1\rangle\big)\\
&\quad \times \big(\cos(\theta+\pi/2)|0\rangle + i\sin(\theta+\pi/2)|1\rangle\big)\Big)/\sqrt{2}
\end{aligned}
$$

$$
\begin{aligned}
&= \big(\big(\cos(\theta)ZX|0\rangle - i\sin(\theta)ZX|1\rangle\big)\big(\cos(\theta)|0\rangle + i\sin(\theta)|1\rangle\big)\\
&\quad + \big(\cos(\theta+\pi/2)ZX|0\rangle - i\sin(\theta+\pi/2)ZX|1\rangle\big)\\
&\quad \times \big(\cos(\theta+\pi/2)|0\rangle + i\sin(\theta+\pi/2)|1\rangle\big)\big)/\sqrt{2}\\
&= \big(\big(-\cos(\theta)|1\rangle - i\sin(\theta)|0\rangle\big)\big(\cos(\theta)|0\rangle + i\sin(\theta)|1\rangle\big)\\
&\quad + \big(-\cos(\theta+\pi/2)|1\rangle - i\sin(\theta+\pi/2)|0\rangle\big)\\
&\quad \times \big(\cos(\theta+\pi/2)|0\rangle + i\sin(\theta+\pi/2)|1\rangle\big)\big)/\sqrt{2}\\
&= \big(\big(-\cos(\theta)|1\rangle - i\sin(\theta)|0\rangle\big)\big(\cos(\theta)|0\rangle + i\sin(\theta)|1\rangle\big)\\
&\quad + \big(\sin(\theta)|1\rangle - i\cos(\theta)|0\rangle\big)\big(-\sin(\theta)|0\rangle + i\cos(\theta)|1\rangle\big)\big)/\sqrt{2}\\
&= \big(-\cos(\theta)^2|10\rangle - i\sin(\theta)\cos(\theta)|00\rangle - i\cos(\theta)\sin(\theta)|11\rangle + \sin(\theta)^2|01\rangle\\
&\quad - \sin(\theta)^2|10\rangle + i\sin(\theta)\cos(\theta)|00\rangle + i\cos(\theta)\sin(\theta)|11\rangle + \cos(\theta)^2|01\rangle\big)/\sqrt{2}\\
&= \big(|01\rangle - |10\rangle\big)/\sqrt{2}. \qquad \text{(B.13)}
\end{aligned}
$$

3. *Entanglement in the x-y plane of Fig.* A1(b), *where* $\theta = 0°$, *and* ϕ *can vary freely:* Then the model of qubit results,

$$|\psi(0°,\phi)\rangle = \cos(0°)|0\rangle + e^{i\phi}\sin(0°)|1\rangle = |0\rangle. \qquad \text{(B.14)}$$

Thus, we arrive at the four Bell states [45] of entanglement in the most direct way,

$$|\beta_{00}\rangle = \big(|00\rangle + |11\rangle\big)/\sqrt{2}, \qquad \text{(B.15)}$$

$$
\begin{aligned}
|\beta_{01}\rangle &= \big(X|00\rangle + X|11\rangle\big)/\sqrt{2}\\
&= \big(|X00\rangle + |X11\rangle\big)/\sqrt{2}\\
&= \big(|10\rangle + |01\rangle\big)/\sqrt{2}\\
&= \big(|01\rangle + |10\rangle\big)/\sqrt{2}, \qquad \text{(B.16)}
\end{aligned}
$$

$$
\begin{aligned}
|\beta_{10}\rangle &= \big(Z|00\rangle + Z|11\rangle\big)/\sqrt{2}\\
&= \big(|Z00\rangle + |Z11\rangle\big)/\sqrt{2}\\
&= \big(|00\rangle - |11\rangle\big)/\sqrt{2}, \qquad \text{(B.17)}
\end{aligned}
$$

$$
\begin{aligned}
|\beta_{11}\rangle &= \big(ZX|00\rangle + ZX|11\rangle\big)/\sqrt{2}\\
&= \big(|ZX00\rangle + |ZX11\rangle\big)/\sqrt{2}\\
&= \big(|Z10\rangle + |Z01\rangle\big)/\sqrt{2}\\
&= \big(-|10\rangle + |01\rangle\big)/\sqrt{2}\\
&= \big(|01\rangle - |10\rangle\big)/\sqrt{2}. \qquad \text{(B.18)}
\end{aligned}
$$

Appendix C: Ambiguous and complete quantum teleportation protocol

According to the timeline of Fig. 1, it is possible to move from left to right in that figure until the ambiguity manifests itself. Then, we will now calculate the wave function at each instant:

- At t_0, we have:

$$\begin{aligned}|\psi(t_0)\rangle &= |\psi\rangle|\beta_{00}\rangle \\ &= \big(\alpha|0\rangle + \beta|1\rangle\big)\big(|00\rangle + |11\rangle\big)/\sqrt{2} \\ &= \big(\alpha|000\rangle + \beta|100\rangle + \alpha|011\rangle + \beta|111\rangle\big)/\sqrt{2}. \end{aligned} \tag{C.1}$$

- Before t_1, a CNOT gate in applied between qubits $q[0]$ and $q[1]$, then:

$$\begin{aligned}|\psi(t_1)\rangle &= (CNOT \otimes I_{2\times 2})|\psi(t_0)\rangle \\ &= \left(\begin{bmatrix}1&0&0&0\\0&1&0&0\\0&0&0&1\\0&0&1&0\end{bmatrix} \otimes \begin{bmatrix}1&0\\0&1\end{bmatrix}\right)\big(\alpha|000\rangle + \beta|100\rangle + \alpha|011\rangle + \beta|111\rangle\big)/\sqrt{2} \\ &= \begin{pmatrix}1&0&0&0&0&0&0&0\\0&1&0&0&0&0&0&0\\0&0&1&0&0&0&0&0\\0&0&0&1&0&0&0&0\\0&0&0&0&0&0&1&0\\0&0&0&0&0&0&0&1\\0&0&0&0&1&0&0&0\\0&0&0&0&0&1&0&0\end{pmatrix}\begin{bmatrix}\alpha/\sqrt{2}\\0\\0\\\alpha/\sqrt{2}\\\beta/\sqrt{2}\\0\\0\\\beta/\sqrt{2}\end{bmatrix} = \begin{bmatrix}\alpha/\sqrt{2}\\0\\0\\\alpha/\sqrt{2}\\0\\\beta/\sqrt{2}\\\beta/\sqrt{2}\\0\end{bmatrix} \\ &= \big(\alpha|000\rangle + \beta|101\rangle + \alpha|011\rangle + \beta|110\rangle\big)/\sqrt{2}, \end{aligned} \tag{C.2}$$

where $\otimes$ means Kronecker's product [45], which is generally omitted from the equations so as not to complicate the notation.

- Before t_2, a Hadamard (H) gate is applied to qubit $q[0]$:

$$\begin{aligned}|\psi(t_2)\rangle &= (H \otimes I_{4\times 4})|\psi(t_1)\rangle \\ &= \left(\begin{bmatrix}1/\sqrt{2}&1/\sqrt{2}\\1/\sqrt{2}&-1/\sqrt{2}\end{bmatrix} \otimes \begin{bmatrix}1&0&0&0\\0&1&0&0\\0&0&1&0\\0&0&0&1\end{bmatrix}\right) \\ &\quad \times \big(\alpha|000\rangle + \beta|101\rangle + \alpha|011\rangle + \beta|110\rangle\big)/\sqrt{2} \\ &= \begin{bmatrix}1/\sqrt{2}&0&0&0&1/\sqrt{2}&0&0&0\\0&1/\sqrt{2}&0&0&0&1/\sqrt{2}&0&0\\0&0&1/\sqrt{2}&0&0&0&1/\sqrt{2}&0\\0&0&0&1/\sqrt{2}&0&0&0&1/\sqrt{2}\\1/\sqrt{2}&0&0&0&-1/\sqrt{2}&0&0&0\\0&1/\sqrt{2}&0&0&0&-1/\sqrt{2}&0&0\\0&0&1/\sqrt{2}&0&0&0&-1/\sqrt{2}&0\\0&0&0&1/\sqrt{2}&0&0&0&-1/\sqrt{2}\end{bmatrix} \end{aligned}$$

$$
\times \begin{bmatrix} \alpha/\sqrt{2} \\ 0 \\ 0 \\ \alpha/\sqrt{2} \\ 0 \\ \beta/\sqrt{2} \\ \beta/\sqrt{2} \\ 0 \end{bmatrix} = \begin{bmatrix} \alpha/2 \\ \beta/2 \\ \beta/2 \\ \alpha/2 \\ \alpha/2 \\ -\beta/2 \\ -\beta/2 \\ \alpha/2 \end{bmatrix}
$$

$$
\begin{aligned}
&= \big(\alpha|000\rangle + \beta|001\rangle + \beta|010\rangle + \alpha|011\rangle + \alpha|100\rangle - \beta|101\rangle \\
&\quad - \beta|110\rangle + \alpha|111\rangle\big)/2 \\
&= \big(|00\rangle\big(\alpha|0\rangle + \beta|1\rangle\big) + |01\rangle\big(\alpha|1\rangle + \beta|0\rangle\big) + |10\rangle\big(\alpha|0\rangle - \beta|1\rangle\big) \\
&\quad + |11\rangle\big(\alpha|1\rangle - \beta|0\rangle\big)\big)/2 \\
&= \big(|00\rangle X^0Z^0\big(\alpha|0\rangle + \beta|1\rangle\big) + |01\rangle X^1Z^0\big(\alpha|0\rangle + \beta|1\rangle\big) \\
&\quad + |10\rangle X^0Z^1\big(\alpha|0\rangle + \beta|1\rangle\big) + |11\rangle X^1Z^1\big(\alpha|0\rangle + \beta|1\rangle\big)\big)/2 \\
&= \big(|00\rangle X^0Z^0|\psi\rangle + |01\rangle X^1Z^0|\psi\rangle + |10\rangle X^0Z^1|\psi\rangle + |11\rangle X^1Z^1|\psi\rangle\big)/2 \\
&\equiv \big(|\beta_{00}\rangle X^0Z^0|\psi\rangle + |\beta_{01}\rangle X^1Z^0|\psi\rangle + |\beta_{10}\rangle X^0Z^1|\psi\rangle + |\beta_{11}\rangle X^1Z^1|\psi\rangle\big)/2, \qquad \text{(C.3)}
\end{aligned}
$$

where X, and Z are the Pauli's matrices known as inverter and phase gates, respectively [45], and that were defined in Appendix B.

Appendix D: Non-ambiguous and simplified quantum teleportation protocol

According to the timeline of Fig. 2, we have:

- At t_0, and considering Equations (8), (9), (B.4a), and (B.4b), yields,

$$
\begin{aligned}
|\psi(t_0)\rangle &= |\beta_{00}\rangle \\
&= \big(\big|\psi(\theta,0^\circ)\big\rangle\big|\psi(\theta,0^\circ)\big\rangle + \big|\psi(\theta+\pi/2,0^\circ)\big\rangle\big|\psi(\theta+\pi/2,0^\circ)\big\rangle\big)/\sqrt{2} \\
&= \big(\big(\cos(\theta)|0\rangle + \sin(\theta)|1\rangle\big) \otimes \big(\cos(\theta)|0\rangle + \sin(\theta)|1\rangle\big) \\
&\quad + \big(\cos(\theta+\pi/2)|0\rangle + \sin(\theta+\pi/2)|1\rangle\big) \\
&\quad \otimes \big(\cos(\theta+\pi/2)|0\rangle + \sin(\theta+\pi/2)|1\rangle\big)\big)/\sqrt{2} \\
&= \left(\begin{bmatrix} \cos(\theta) \\ \sin(\theta) \end{bmatrix} \otimes \begin{bmatrix} \cos(\theta) \\ \sin(\theta) \end{bmatrix} + \begin{bmatrix} \cos(\theta+\pi/2) \\ \sin(\theta+\pi/2) \end{bmatrix} \otimes \begin{bmatrix} \cos(\theta+\pi/2) \\ \sin(\theta+\pi/2) \end{bmatrix}\right)/\sqrt{2} \\
&= \left(\begin{bmatrix} \cos(\theta) \\ \sin(\theta) \end{bmatrix} \otimes \begin{bmatrix} \cos(\theta) \\ \sin(\theta) \end{bmatrix} + \begin{bmatrix} -\sin(\theta) \\ \cos(\theta) \end{bmatrix} \otimes \begin{bmatrix} -\sin(\theta) \\ \cos(\theta) \end{bmatrix}\right)/\sqrt{2} \\
&= \frac{1}{\sqrt{2}} \begin{bmatrix} \cos(\theta)^2 + \sin(\theta)^2 \\ \cos(\theta)\sin(\theta) - \sin(\theta)\cos(\theta) \\ \sin(\theta)\cos(\theta) - \cos(\theta)\sin(\theta) \\ \sin(\theta)^2 + \cos(\theta)^2 \end{bmatrix}
\end{aligned}
$$

$$= \frac{1}{\sqrt{2}} \begin{bmatrix} 1 \\ 0 \\ 0 \\ 1 \end{bmatrix} = \big(|00\rangle + |11\rangle\big)/\sqrt{2}, \tag{D.1}$$

which verifies the internal constitution of $|\beta_{00}\rangle$ as a function of the selected qubit model of Equation (8). On the other hand, the θ angle of Fig. 2 is not a qubit, but a classical input acting on a rotatable polarizer $P(\theta)$ in the form of a voltage proportional to the chosen angle. Furthermore, the rotatable polarizer can be implemented directly [41],

$$P(\theta) = \begin{bmatrix} \cos(\theta)^2 & \cos(\theta)\sin(\theta) \\ \sin(\theta)\cos(\theta) & \sin(\theta)^2 \end{bmatrix}, \tag{D.2}$$

or through the following configuration based on two electro-optical-modulators (EOMs) [42],

$$\begin{aligned} P(\theta) &= R(\theta)P(0^\circ)R(\theta)^T \\ &= \begin{bmatrix} \cos(\theta) & -\sin(\theta) \\ \sin(\theta) & \cos(\theta) \end{bmatrix} \begin{bmatrix} 1 & 0 \\ 0 & 0 \end{bmatrix} \begin{bmatrix} \cos(\theta) & \sin(\theta) \\ -\sin(\theta) & \cos(\theta) \end{bmatrix} \\ &= \begin{bmatrix} \cos(\theta) & -\sin(\theta) \\ \sin(\theta) & \cos(\theta) \end{bmatrix} \begin{bmatrix} \cos(\theta) & \sin(\theta) \\ 0 & 0 \end{bmatrix} \\ &= \begin{bmatrix} \cos(\theta)^2 & \cos(\theta)\sin(\theta) \\ \sin(\theta)\cos(\theta) & \sin(\theta)^2 \end{bmatrix}, \end{aligned} \tag{D.3}$$

where $(\bullet)^T$ means *transpose of* $(\bullet)$, each $R(\theta)$ is implemented with an $EOM(\theta)$, and $P(0^\circ)$ is a completely fixed horizontal polarizer. It is also possible to implement the rotatable polarizer by means of two half-wave plates (HWP), but for an angle equal to half θ,

$$\begin{aligned} P(\theta) &= R(\theta)P(0^\circ)R(\theta)^T \\ &= \begin{bmatrix} \cos(2\theta) & \sin(2\theta) \\ \sin(2\theta) & -\cos(2\theta) \end{bmatrix} \begin{bmatrix} 1 & 0 \\ 0 & 0 \end{bmatrix} \begin{bmatrix} \cos(2\theta) & \sin(2\theta) \\ \sin(2\theta) & -\cos(2\theta) \end{bmatrix} \\ &= \begin{bmatrix} \cos(2\theta) & \sin(2\theta) \\ \sin(2\theta) & -\cos(2\theta) \end{bmatrix} \begin{bmatrix} \cos(2\theta) & \sin(2\theta) \\ 0 & 0 \end{bmatrix} \\ &= \begin{bmatrix} \cos(2\theta)^2 & \cos(2\theta)\sin(2\theta) \\ \sin(2\theta)\cos(2\theta) & \sin(2\theta)^2 \end{bmatrix}. \end{aligned} \tag{D.4}$$

The difference between θ and 2θ between Equations (D.3) and (D.4) is due to the fact that in the case of the HWPs we achieve the same rotation as with half the angle considered in the EOMs. Otherwise, both possible implementations of the rotatable polarizer, i.e., via EOM, Equation (D.3), or via HWP, Equation (D.4), are equally effective; We only have to take into account the context in which the rotatable polarizer will be used, that is, for laboratory experiments, or quantum communications. If the case is the latter, two critical aspects must be considered:

1. the speed of switching between angles, and
2. the delay generated by the EOM-Ph+EOM and HWP+Ph+HWP blocks.

For these two reasons, i.e., lower speed of switching between angles and delay, we have decided to carry out the implementations of Sect. 3 using the EOM-Ph+EOM block.

Therefore, taking into account Equations (D.2) and (D.3), we continue with the timeline of Fig. 2, in such a way that:

• At t_1:

$$
\begin{aligned}
|\psi(t_1)\rangle &= \big(P(\theta)\otimes I_{2\times 2}\big)|\beta_{00}\rangle \\
&= \left(\begin{bmatrix} \cos(\theta)^2 & \cos(\theta)\sin(\theta) \\ \sin(\theta)\cos(\theta) & \sin(\theta)^2 \end{bmatrix} \otimes \begin{bmatrix} 1 & 0 \\ 0 & 1 \end{bmatrix}\right) \frac{1}{\sqrt{2}} \begin{bmatrix} 1 \\ 0 \\ 0 \\ 1 \end{bmatrix} \\
&= \begin{bmatrix} \cos(\theta)^2 & 0 & \cos(\theta)\sin(\theta) & 0 \\ 0 & \cos(\theta)^2 & 0 & \cos(\theta)\sin(\theta) \\ \sin(\theta)\cos(\theta) & 0 & \sin(\theta)^2 & 0 \\ 0 & \sin(\theta)\cos(\theta) & 0 & \sin(\theta)^2 \end{bmatrix} \frac{1}{\sqrt{2}} \begin{bmatrix} 1 \\ 0 \\ 0 \\ 1 \end{bmatrix} \\
&= \frac{1}{\sqrt{2}} \begin{bmatrix} \cos(\theta)^2 \\ \cos(\theta)\sin(\theta) \\ \sin(\theta)\cos(\theta) \\ \sin(\theta)^2 \end{bmatrix} \\
&= \frac{1}{\sqrt{2}} \begin{bmatrix} \cos(\theta) \\ \sin(\theta) \end{bmatrix} \otimes \begin{bmatrix} \cos(\theta) \\ \sin(\theta) \end{bmatrix} \\
&= \frac{(\cos(\theta)|0\rangle + \sin(\theta)|1\rangle) \otimes (\cos(\theta)|0\rangle + \sin(\theta)|1\rangle)}{\sqrt{2}} \\
&= \frac{|\psi(\theta)\rangle \otimes |\psi(\theta)\rangle}{\sqrt{2}}.
\end{aligned}
\tag{D.5}
$$

Appendix E: Difference between a cloning machine and an induction, projection, and collapse (IPC) machine

Figure E1 shows the difference between a cloning machine (CloM) and an induction, projection, and collapse machine (IPCM). In the first case, we have $|\psi(\theta,\phi)\rangle \otimes |\psi(\theta,\phi)\rangle = CloM(|\psi(\theta,\phi)\rangle)$, see Fig. E1(a), that is, enter a state $|\psi(\theta,\phi)\rangle$ and an ancilla $|0\rangle$ is incorporated internally, which is not shown in the figure. The machine tries to clone the incoming state in such a way as to obtain two states identical to the incoming one at its output. This machine is impossible to implement, and this impossibility is demonstrated in the No-Cloning Theorem [47]. In the second case, we have $|\psi(\theta,\phi)\rangle \otimes |\psi(\theta,\phi)\rangle = IPCM(\theta,\phi)$, see Fig. E1(b), such that given an angle θ as a variable independent and another ϕ angle as a parameter (ceteris paribus), the machine generates an entangled pair from the θ angle according to the qubit model of Equation (8) and the resulting base of Equation (9). This is an induction of a Bell basis from a qubit model dependent on the incoming θ angle to one of the machine qubits. The action of a polarizer at a θ angle on that qubit acts as a weak measurement, which projects the state selected by the polarizer to the second qubit. This

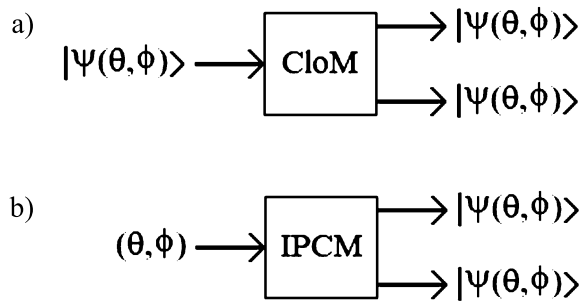

Figure E1 Difference between (**a**) a cloning machine (CloM), and (**b**) an induction, projection, and collapse machine (IPCM). In the first case (CloM), there is a clone of the incoming state $|\psi(\theta,\phi)\rangle$, while in the second case (IPCM) the fixed angle θ (since ϕ is a parameter, *ceteris paribus*) in the rotatable polarizer collapses the wavefunction into two identical outcomes $|\psi(\theta,\phi)\rangle$

constitutes a collapse of the shared wavefunction to one of two possible outcomes resulting from such a collapse, that is to say, $|\psi(\theta,\phi)\rangle \otimes |\psi(\theta,\phi)\rangle$, or $|\psi(\theta+\pi/2,\phi)\rangle \otimes |\psi(\theta+\pi/2,\phi)\rangle$, in particular to that of angle θ, that is, those selected by the rotatable polarizer, as we can see in Fig. 2.

In other words, the IPC machine is not a cloning machine, in a broad sense of the word, since an arbitrary state $|\psi(\theta,\phi)\rangle$ to be cloned does not enter explicitly the machine, but an arbitrary angle θ with another angle ϕ as parameter. If the θ angle is known, obviously it is not arbitrary and according to the qubit model of Equation (8), we obtain two identical states at the output of the machine as a function of that angle (based on the mentioned model), that is, it is an indirect clone. Furthermore, if the θ angle is unknown to us, and according to the same qubit model, we will obtain the same result. Therefore, assuming the existence of an underlying state to be cloned, which is indirectly represented by a couple of angles, we can say that the configuration in Fig. E1(b) is an implicit clone machine (in-situ), while the one in Fig. E1(a) is an explicit cloning machine (ex-situ), which we know to be physically unfeasible [47].

Finally, and as another outstanding difference between both machines, CloM does not necessarily imply the intervention of the entanglement, while IPCM involves it as a *sine qua non* condition.

Acknowledgements
M.M. thanks the staff of the Knight Foundation School of Computing and Information Sciences at Florida International University for all their help and support.

Funding
The author has not disclosed any funding.

Availability of data and materials
The experimental data that support the findings of this study are available in Harvard Dataverse with the identifier https://doi.org/10.7910/DVN/LOLQJD.

Declarations

Competing interests
The authors declare no competing interests.

Author contributions
M.M. conceived the idea and fully developed the theory, developed the experiments on the simulator and the optical table, wrote the complete manuscript, prepared figures, and reviewed the manuscript.

Received: 5 February 2023 Accepted: 12 April 2023 Published online: 11 May 2023

References

1. Bennett CH, Brassard G, Crépeau C, Jozsa R, Peres A, Wootters WK. Teleporting an unknown quantum state via dual classic and Einstein-Podolsky-Rosen channels. Phys Rev Lett. 1993;70:1895–9.
2. Ezratty O. Understanding quantum technologies. The quantum energy initiative. Paris: Le Lab Quantique; 2022.
3. Lele A. Quantum technologies and military strategy. Cham: Springer; 2021.
4. Osada A, Yamazaki R, Noguchi A. Introduction to quantum technologies. Singapore: Springer; 2022.
5. Cariolaro G. Quantum communications. New York: Springer; 2015.
6. Pathak A. Elements of quantum computation and quantum communication. Boca Raton: Taylor & Francis; 2013.
7. Mishra VK. An introduction to quantum communication. New York: Momentum Press; 2016.
8. Imre S, Gyongyosi L. Advanced quantum communications: an engineering approach. New York: Wiley; 2012.
9. Bouwmeester D, Pan JW, Mattle K, Eibl M, Weinfurter H, Zeilinger A. Experimental quantum teleportation. Nature. 1997;390:575–9.
10. Boschi D, Branca S, De Martini F, Hardy L, Popescu S. Experimental realization of teleporting an unknown pure quantum state via dual classical and Einstein-Podolski-Rosen channels. Phys Rev Lett. 1998;80:1121–5.
11. Furusawa A, Sørensen JL, Braunstein SL, Fuchs CA, Kimble HJ, Polzik ES. Unconditional quantum teleportation. Science. 1998;282(5389):706–9.
12. Barrett MD, Chiaverini J, Schaetz T, Britton J, Itano WM, Jost JD, Knill E, Langer C, Leibfried D, Ozeri R, Wineland DJ. Deterministic quantum teleportation of atomic qubits. Nature. 2004;429:737–9.
13. Riebe M, Häffner H, Roos CF, Hänsel W, Benhelm J, Lancaster GPT, Körber TW, Becher C, Schmidt-Kaler F, James DFV, Blatt R. Deterministic quantum teleportation with atoms. Nature. 2004;429:734–7.
14. Sherson JF, Krauter H, Olsson RK, Julsgaard B, Hammerer K, Cirac I, Polzik ES. Quantum teleportation between light and matter. Nature. 2006;443:557–60.
15. Yang J, Bao XH, Zhang H, Chen S, Peng CZ, Chen ZB, Pan JW. Experimental quantum teleportation and multi-photon entanglement via interfering narrowband photon sources. Phys Rev A. 2009;80(4):042321.
16. Ma XS, Kropatschek S, Naylor W, Scheidl T, Kofler J, Herbst T, Zeilinger A, Ursin R. Experimental quantum teleportation over a high-loss free-space channel. Opt Express. 2012;20(21):23126–37.
17. van Houwelingen JAW, Beveratos A, Brunner N, Gisin N, Zbinden H. Experimental quantum teleportation with a 3-Bell-state analyzer. Phys Rev A. 2006;74:11.
18. Carlo GG, Benenti G, Casati G. Teleportation in a noisy environment: a quantum trajectories approach. Phys Rev Lett. 2003;91:25.
19. Marzolino U, Buchleitner A. Performances and robustness of quantum teleportation with identical particles. Proc, Math Phys Eng Sci. 2016;472:2185.
20. Hedemann SR. Noise-resistant quantum teleportation, ansibles, and the no-projector theorem. 2016. arXiv:1605.09233.
21. Huo M, Qin J, Cheng J, Yan Z, Qin ZZ, Su XL, Jia XJ, Xie C, Peng K. Deterministic quantum teleportation through fiber channels. Sci Adv. 2018;4:10.
22. Sergienko AV, editor. Quantum communications and cryptography. London: Taylor & Francis; 2006.
23. Kumar N, Agrawal A, Chaurasia BK, Khan RA, editors. Limitations and future applications of quantum cryptography. Hershey: IGI Global; 2021.
24. Liao SK, Cai WQ, Liu WY, Zhang L, Li Y, Ren JG, Yin J, Shen Q, Cao Y, Li ZP, Li LF, Chen XW, Sun LH, Jia JJ, Wu JC, Jiang XJ, Wang JF, Huang YM, Wang Q, Zhou YL, Deng L, Xi T, Ma L, Hu T, Pan JW. Satellite-to-ground quantum key distribution. Nature. 2017;549:43–7.
25. Bedington R, Arrazola JM, Ling A. Progress in satellite quantum key distribution. npj Quantum Inf. 2017;3:30.
26. Sibson P, Erven C, Godfrey M, Miki S, Yamashita T, Fujiwara M, Sasaki M, Terai H, Tanner MG, Natarajan CM, Hadfield RH, O'Brien JL, Thompson MG. Chip-based quantum key distribution. Nat Commun. 2017;8:13984.
27. Lucamarini M, Yuan ZL, Dynes JF, Shields AJ. Overcoming the rate–distance limit of quantum key distribution without quantum repeaters. Nature. 2018;557:400–3.
28. Behera BK, Seth S, Das A, Panigrahi PK. Demonstration of entanglement purification and swapping protocol to design quantum repeater in IBM quantum computer. In: Quantum inf process. vol. 18. 2019. p. 108.
29. Ruihong Q, Ying M. Research progress of quantum repeaters. IOP J Phys: Conf Ser. 2019;1237:052032.
30. Mastriani M. How can a random phenomenon between particles be synchronized instantaneously and independently of the distance between said particles? Opt Quantum Electron. 2022;54:235.
31. Wehner S, Elkouss D, Hanson R. Quantum Internet: a vision for the road ahead. Science. 2018;362(6412):eaam9288.
32. Castelvecchi D. Here's what the quantum internet has in store: physicists say this futuristic, super-secure network could be useful long before it reaches technological maturity. Nat News. 2018.
33. Caleffi M, Cacciapuoti AS, Bianchi G. Quantum Internet: from communication to distributed computing. In: NANOCOM '18: proceedings of the 5th ACM international conference on nanoscale computing and communication. vol. 3. 2018. p. 1–4.
34. Kimble HJ. The quantum Internet. Nature. 2008;453:1023–30.
35. Caleffi M, Chandra D, Cuomo D, Hassanpour S, Cacciapuoti AS. The rise of the quantum Internet. IEEE Comput. 2020;53(06):67–72.
36. Cacciapuoti AS, Caleffi M, Cataliotti FS, Gherardini S, Tafuri F, Bianchi G. The quantum Internet: networking challenges in distributed quantum computing. IEEE Netw. 2020;34(1):137–43.
37. Cacciapuoti AS, Caleffi M, Van Meter R, When HL. Entanglement meets classical communications: quantum teleportation for the quantum Internet. IEEE Trans Commun. 2020;68(6):3808–33.
38. Gyongyosi L, Imre S. Entanglement accessibility measures for the quantum Internet. In: Quantum inf process. vol. 19. 2020. p. 115.
39. Gyongyosi L, Imre S. Entanglement access control for the quantum Internet. In: Quantum inf process. vol. 18. 2019. p. 107.
40. Gyongyosi L, Imre S. Opportunistic entanglement distribution for the quantum Internet. Sci Rep. 2019;9:2219.

41. Liquid Crystal Polarization Rotators. https://www.thorlabs.com/newgrouppage9.cfm?objectgroup_id=10813. Accessed 16 Jan 2023.
42. Free-Space Electro-Optic Modulators. https://www.thorlabs.com/newgrouppage9.cfm?objectgroup_id=2729. Accessed 16 Jan 2023.
43. Einstein A, Podolsky B, Can RN. Quantum-mechanical description of physical reality be considered complete? Phys Rev. 1935;47(10):777–80.
44. Phillips AC. Introduction to quantum mechanics. New York: Wiley; 2003.
45. Nielsen MA, Chuang IL. Quantum computation and quantum information. Cambridge: Cambridge University Press; 2004.
46. Busch P, Lahti P, Pellonpää JP, Ylinen K. Quantum measurement. New York: Springer; 2016.
47. Wootters WK, Zurek WH. A single quantum cannot be cloned. Nature. 1982;299:802–3.
48. Sk R, Baishya A, Behera BK, Panigrahi PK. Experimental realization of quantum teleportation of an arbitrary two-qubit state using a four-qubit cluster state. Quantum Inf Process. 2020;19:87.
49. Free space optical delay line. Thorlabs. https://www.thorlabs.com/newgrouppage9.cfm?objectgroup_id=5521. Accessed 16 Jan 2023.
50. DiCola T. Arduino GPS Clock. https://learn.adafruit.com/arduino-clock. Accessed 16 Jan 2023.
51. Adafruit METRO 328 Fully Assembled – Arduino IDE compatible – ATmega328. https://www.adafruit.com/product/50. Accessed 16 Jan 2023.
52. Boyd RW, Lukishova SG, Zadkov VN, editors. Quantum photonics: pioneering advances and emerging applications. Switzerland: Springer; 2019.
53. Khatri S, Wilde MM. Principles of quantum communication theory: a modern approach. 2020. arXiv:2011.04672.
54. An RM. Introduction to quantum communications networks: or, how shall we communicate in the quantum era? San Rafael: Morgan & Claypool Pub.; 2018.
55. Smith WF, editor. Experimental physics: principles and practice for the laboratory. Boca Raton: CRC Press; 2020.

Publisher's Note